Author version: *J. Geophys. Res. (B: Solid Earth), vol.117; 2012; B04101, 19pp.*

Tectonics of the Ninetyeast Ridge derived from spreading records in adjacent oceanic basins and age constraints of the ridge

Kolluru S. Krishna[1], Honey Abraham[1], William W. Sager[2], Malcolm S. Pringle[3], Frederick Frey[3], Dasari Gopala Rao[4], Oleg V. Levchenko[5]

[1] National Institute of Oceanography, Council of Scientific and Industrial Research, Dona Paula, Goa – 403004, India
[2] Department of Oceanography, Texas A&M University, College Station, TX 77843-3146, USA
3 Department of Earth and Planetary Sciences, Massachusetts Institute of Technology, Cambridge, MA 02139 USA
[4] Department of Geology, Osmania University, Hyderabad – 500007, India
[5] Shirshov Institute of Oceanology, Russian Academy of Sciences, Moscow 117997, Russian Federation

Abstract

Analysis of new and existing geophysical data for the Central Indian and Wharton Basins of the Indian Ocean was used to understand the formation and evolution of the Ninetyeast Ridge (NER), especially its relationship to the Kerguelen hot spot and the Wharton spreading ridge. Satellite gravity data and magnetic anomalies 34 through 19 define crustal isochrons and show fracture zones striking ~N 5˚E. One of these, at 89°E, crosses the ~N 10˚E trending-NER, impacting the NER morphology. From 77 to 43 Ma the NER lengthened at a rate of ~118 km/Myr, twice that of the ~48-58 km/Myr accretion rate of adjacent oceanic crust. This difference can be explained by southward jumps of the Wharton spreading ridge towards the hot spot, which transferred portions of crust from the Antarctic plate to the Indian plate, lengthening the NER. Magnetic anomalies document a small number of large spreading ridge jumps in the ocean crust immediately to the west of the NER, especially two leaving observable 65 and 42 Ma fossil spreading ridges. In contrast, complex magnetic anomaly progressions and morphology imply that smaller spreading ridge jumps occurred at more frequent

intervals beneath the NER. Comparison of the NER dates and magnetic anomaly ages implies that the hot spot first emplaced NER volcanoes on the Indian plate at a distance from the Wharton Ridge, but as the northward-drifting spreading ridge approached the hot spot, the two interacted, keeping later NER volcanism near the spreading ridge crest by spreading center jumps.

Key Words: Ninetyeast Ridge, Kerguelen hot spot, Ridge-hot spot interactions, Ridge Jumps, Ridge Migration

1. Introduction

The Ninetyeast Ridge (NER), one of the longest linear volcanic features on the Earth, extends ~5600 km in the N-S direction from 34°S to 17°N (Figure 1). Its southern part intersects the E-W trending Broken Ridge and the northern part (north of 10°N) is entirely buried under thick Bengal Fan sediments (Curray et al., 1982; Gopala Rao et al., 1997; Michael and Krishna, 2011), beneath which it converges upon the Andaman arc at about 17°N (Subrahmanyam et al., 2008). The ridge has an average width of 200 km and elevation of more than 2 km along most of its length (Sclater and Fisher, 1974; Fisher et al., 1982; Krishna et al., 1995, 2001a). The NER is often asymmetric in cross-section and ranges from low relief to high relief seamounts and linear ridge segments with some portions having a flat-topped morphology (Figure 2). Although numerous explanations have been proposed for the formation of the NER, it is widely accepted that the ridge was formed by Kerguelen hot spot volcanism when the hot spot was located beneath the Indian plate during the late Cretaceous and early Cenozoic (Peirce, 1978; Peirce, Weissel et al., 1989; Royer et al., 1991). This hypothesis is supported by

new geochronology data generated for NER core samples from DSDP Leg 26 and ODP Leg 121 (Pringle et al., 2008), which show that the southern ridge is 43 Ma in age at DSDP Site 254 near the Broken Ridge and 77 Ma in age at ODP Site 758 near the north end of the NER and with a remarkably linear age progression in between (Figures 3a, b).

When compared to seafloor spreading in adjacent Central Indian and Wharton basins as delineated by seafloor spreading magnetic anomalies (e.g. Krishna et al., 1995, 1999), the new geochronology data (Pringle et al., 2008) reveal that the volcanic propagation rate (~118 km/ Myr) of the NER is double that of the half-spreading rates (48-58 km/ Myr) of the adjacent oceanic basins and, as a result, the NER is ~11° longer than the length of Indian plate created contemporaneously (Krishna et al., 1999). Previously Royer et al. (1991) and Krishna et al. (1995, 1999) have provided an explanation that the Wharton spreading ridge segments jumped southward several times, transferring lithosphere from Antarctic plate to the Indian plate. But the timing, location of the hot spot, and extent of these ridge jumps are uncertain because magnetic lineations near the NER are complex and magnetic data in the region are sparse.

In this study we compiled and modeled magnetic anomaly profile data from the NER and adjacent basins (Figures 3a and b) and examined the implications of newly available geochronology data from DSDP Leg 22 and ODP Leg 121 cores (Pringle et al., 2008). The geophysical data are mainly utilized for identification of magnetic patterns including fracture zones (FZs) and fossil ridge segments, of both the Wharton and Central Indian basins adjacent to the NER. With the derived tectonic constraints

and geochronology data, we propose a model for interactions between the Wharton spreading center and the Kerguelen hot spot during the emplacement of the NER. Finally we discuss the mechanisms of NER accretion and why its length is much longer compared to that of the adjacent normal oceanic lithosphere formed during the same time interval.

2. NER Tectonic Setting

Major plate reorganizations of Indian Ocean seafloor spreading occurred at ~90 Ma and ~42 Ma, moving the Kerguelen hot spot alternately beneath the Indian and Antarctic plates, respectively (Liu et al., 1983). Initially, at approximately 120 Ma, the hot spot was beneath the Antarctic plate, leading to the formation of the southern and central parts of the Kerguelen Plateau and the Broken Ridge (Coffin et al., 2002). The first major plate reorganization, at ~90 Ma, placed the hot spot beneath the Indian plate and resulted in the accretion of the world's largest linear aseismic ridge, termed the NER. The second major plate reorganization, at ~42 Ma, relocated the hot spot beneath the Antarctic plate and resulted in the accretion of the Northern Kerguelen Plateau, including the Kerguelen Archipelago, and Heard and McDonald Islands (Coffin et al., 2002) since that time. It has been thought that during the formation of the NER, the Kerguelen hot spot was mostly located north of spreading ridge-segments that were part of the western extremity of the Wharton Ridge, which separated the Indian and Australian plates and was connected to the India-Antarctica Ridge through the 86°E transform fault (Krishna et al., 1995, 1999). Concurrently with the NER emplacement, the adjacent Wharton and Central Indian basins were also formed by the spreading of

104 the Wharton and India-Antarctica ridges, respectively (Liu et al., 1983; Royer and
105 Sandwell, 1989; Royer et al., 1991; Krishna et al., 1995, 1999). After the ~42 Ma plate
106 reorganization, the Wharton spreading ridge effectively disappeared as the Southeast
107 Indian Ridge formed, and the Indian and Australian plates merged together to form a
108 single Indo-Australian plate (Liu et al., 1983; Krishna et al., 1995).
109
110 During Neogene time, a large diffuse plate boundary has formed in the central Indian
111 Ocean, breaking the major Indo-Australian plate into three smaller component plates -
112 Indian, Australian, and Capricorn plates (Royer and Gordon, 1997; Gordon et al.,
113 1998). Almost the entire NER resides within this zone of complex deformation.
114 Seismic results from Bengal Fan sediments reveal that the lithosphere within the
115 boundary to the west of the NER displays reverse faulting (5–10-km-spaced faults) and
116 long-wavelength (100–300 km) folding (Weissel et al., 1980; Bull, 1990; Chamot-
117 Rooke et al., 1993; Krishna et al., 1998, 2001b). Using seismic stratigraphy and plate
118 rotations, Krishna et al. (2009a) and Bull et al. (2010) subsequently determined that the
119 lithospheric convergence began at 18-14 Ma within this plate boundary. Recent seismic
120 results from the NER suggest that the ridge is dissected by numerous faults and
121 experiencing ongoing deformation activity (Sager et al., 2010). Furthermore, the ridge
122 is thought to be a structural partition that separates different styles of deformation in the
123 Central Indian and Wharton basins (Deplus et al., 1998; Delescluse and Chamot-Rooke,
124 2007). Despite this ongoing tectonism, the overall deformation of the diffuse
125 boundaries is small and thus can be ignored for our study of late Cretaceous and early
126 Cenozoic plate boundary motions.
127

NER morphology is complex and varies along its length (Fisher et al., 1982; Krishna et al., 2001a; Sager et al., 2010). The southern ridge, south of 11°S, is tall, nearly continuous, and often highly asymmetric with a steep eastern slope and low western slope. In contrast, the ridge north of ~3°S consists of a series of mostly individual, large volcanoes with more symmetric cross-sections. In between, the ridge is low with a combination of small linear segments and seamounts (Krishna et al., 2001a). The position of the Kerguelen hot spot with respect to the Wharton spreading centers, the strike of oceanic fracture zones, plate motions, hot spot drift, variable hot spot magma output, and deformation-related faults are all factors that have been implicated as controls on the morphology of the NER (e.g., Royer et al., 1991).

3. Geophysical and Geological Data

An international scientific expedition was carried out onboard R/V *Roger Revelle* (KNOX06RR) during the year 2007 over the NER (Figure 2). During the cruise multibeam bathymetry, magnetic and gravity data, and 10-fold multichannel seismic reflection profiles, were acquired in the vicinity of ODP Site 758, DSDP Sites 216, 214 and 253 and at locations 6-8°S and 19°S. In addition to the geophysical data, basaltic rocks were also dredged at 22 sites along the NER (see Sager et al., 2007 for locations). Magnetic data utilized in this study were gathered from the KNOX06RR cruise, NGDC (National Geophysical Data Center) and NIO (National Institute of Oceanography) databases and the Trans Indian Ocean Geotraverse (TIOG) program (Table 1; Krishna et al., 1995). In addition we used newly determined $^{40}Ar/^{39}Ar$ radiometric ages (Pringle et al., 2008) of basaltic core samples from DSDP Sites 214, 216, 254 and ODP Sites 756-758 along the NER (Figures 3a, b).

4. Magnetic Anomaly Pattern of the Central Indian and Wharton Basins adjacent to the Ninetyeast Ridge

Magnetic anomaly profile data adjacent to the NER are plotted along ship-tracks and shown in Figures 3a and b. The data are overlaid on satellite free-air gravity data (Sandwell and Smith, 1997) in order to constrain precise positions of fracture zones (FZ), thereby constraining extrapolation of the magnetic lineations. The satellite gravity image clearly shows the presence of a number of nearly N-S trending narrow gravity features, indicating the signatures of FZ created during the northward movement of the Indian plate. From these gravity features, we have traced ten FZ between 80° and 97°E longitudes (Figures 3a and 3b). They trend in the N5°E direction, while the NER trends ~N10°E, consequently the 89°E FZ crosses the NER obliquely from east to west between 15°S and 10°S latitudes (Figures 3a and 3b). Magnetic anomalies are, in general, well developed with moderate amplitudes except over the NER and on its immediate east side (Figures 3a, 3b, 4a, 4b, and 4c). In particular between the 89°E FZ and 94°E FZ, the anomalies are modestly developed with lower amplitudes (Figures 3a, 3b, and 4b). The anomalies within this corridor seem to be subdued because of excessive seafloor undulations created by oceanic fracture zones, strike-slip displacements and vertical faulting (Pilipenko, 1996; Krishna et al., 2001a).

Earlier magnetic anomaly identifications from both the Central Indian and Wharton basins (Peirce, 1978; Liu et al., 1983; Pierce and Weissel et al., 1989; Royer et al., 1991; Krishna et al., 1995, 2009b; Krishna and Gopala Rao, 2000) were considered to

176 determine the spreading rates and magnetic polarity chronology for the calculation of
177 synthetic magnetic anomaly profiles. Half-spreading rates ranging from 2.3 to 8.5
178 cm/yr and geomagnetic polarity timescale (Cande and Kent, 1995) for the period from
179 Late Cretaceous to early Tertiary were used to create synthetic magnetic anomaly
180 models (shown in Figures 4a, 4b, and 4c). Following the anomaly pattern within the
181 study area (west of the 86°E FZ, east of the 90°E FZ, and the region in between) three
182 magnetic models were generated using the Matlab based MODMAG algorithm
183 (Mendel et al., 2005) and correlated to the magnetic anomaly profiles for identification
184 of seafloor spreading magnetic anomalies, thereby assigning ages to the oceanic crust.
185 The magnetic anomaly sequences in model profiles, particularly anomalies 30 through
186 32n.2 and 21 through 24n.2, have characteristic shapes (see Figures 4a, 4b and 4c)
187 generated by a unique arrangement of short-period geomagnetic polarity reversals. We
188 used these distinctive anomaly shapes and patterns as reference picks for the correlation
189 of observed anomalies to model profiles. With this approach most of our anomaly
190 correlations have gained reasonably high confidence.

191

192 A comparison of the observed magnetic anomaly data of both the Central Indian and
193 Wharton basins with synthetic model profiles (Figures 4a, 4b and 4c) leads to the
194 identification of seafloor spreading anomalies 19 through 34, several fossil ridge
195 segments, and a number of nearly N-S oriented FZ along 84°E, 85°E, 86°E, 89°E,
196 90°E, 92°E, 94°E, and 96°E longitudes. It is observed that half-spreading rates are
197 significantly reduced, as low as 2.9 and 2.3 cm/yr, close to the end-phase of ridge
198 segments at anomalies 30 and 19, respectively (Figures 4b and 4c). The ridge segments
199 that ceased at anomaly 19 were part of the cessation of the entire Wharton spreading

200 system, thereby contributing to the second major plate reorganization in the Indian
201 Ocean and unification of Indian and Australian plates into a single major lithospheric
202 plate. This event is thought to be a result of occurrence of continent-continent collision
203 between India and Asia (Liu et al., 1983; Patriat and Segoufin, 1988). In regions to the
204 west of the 86°E FZ and east of the NER, spreading anomalies 19 through 34 are
205 identified with confidence and correlated with the anomaly picks from profile to profile
206 (Figures 4a and 4b). To the west of the 86°E FZ magnetic lineations from 26 to 23n.1
207 are offset approximately along the 84°E and 85°E longitudes in a right-lateral sense by
208 about 90 and 45 km, respectively, revealing the presence of oceanic fracture zones,
209 termed as the 84°E FZ and 85°E FZ (Figures 5a and 5b). Likewise to the east of the
210 NER the magnetic lineations from 32n.1 to 19 show large offsets approximately along
211 90°E, 92°E and 94°E longitudes in the opposite (left-lateral) sense by about 840, 820
212 and 150 km, respectively, revealing the presence of oceanic fracture zones, identified as
213 the 90°E FZ, 92°E FZ and 94°E FZ (Figures 5a and 5b).

214

215 By comparison of the magnetic anomalies from profiles Wilkes815 (Pr. 9), sk82-02 (Pr.
216 3), dsdp22gc (Pr. 22), sk124-12 (Pr. 21), C1709 (Pr. 23), sk124-10 (Pr. 20), inmd06mv
217 (Pr. 14), wilkes815 (Pr. 24), circ05AR-B (Pr. 46), tiog15 (Pr. 48), tiog16 (Pr. 49),
218 circ05AR-C (Pr. 70), RC1402 (Pr. 32) and Wilkes907 (Pr. 71) with the synthetic
219 magnetic model (Figure 4c), we identify symmetric pairs of anomaly sequences 30
220 through 32n.2 and 20 through 23n.1 on either side of anomaly signatures presumed to be
221 associated with fossil ridge segments. These sequences evolved by the abandonment of
222 ridge segments soon after anomaly 30 and at anomaly 19, respectively. In addition we
223 identify anomalies 26 to 29 (increasing age towards the north) in between the aforesaid

anomaly sequences, and anomalies 24n.2 and 25 on the south side of the younger anomaly sequence (Figures 4c, 5a, and 5b). Furthermore, minor dislocations, <50 km, are noted at two places, particularly in anomalies from 26 to 29 and 20 to 23n.2, and this led to recognition of smaller second-order fracture zones whose continuation is not observed in anomalies older than 30 (Figures 4c, 5a, and 5b). This suggests that these two fracture zones may have originated after magnetic anomaly 30 and continued up to anomaly 19. Thus the magnetic pattern in the corridor between the 86°E FZ and the NER has been disrupted by fracture zones and spreading ridge jumps, and as a result the magnetic pattern has become more complex in comparison to that of other regions west of the 86°E FZ and east of the NER. Previous studies have noted complex magnetic patterns west of the NER (Royer et al., 1991; Krishna et al., 1995; Krishna and Gopala Rao, 2000) and in the Wharton Basin (Liu et al., 1983) in broader perspective. In this study we generated more accurate magnetic anomaly maps for the basinal regions on both sides of much of the NER using up-to-date available magnetic anomaly profile data and satellite gravity anomaly data (Figures 5a and 5b), providing tighter constraints on the evolution of the NER and the interaction of the hot spot with spreading ridge segments.

Ages of the oceanic crust obtained from the magnetic lineations agree with ages of rock samples recovered at DSDP Site 215 in the Central Indian Basin and basal sediments sampled from DSDP Site 213 in the Wharton Basin, giving confidence in the anomaly identifications. The rock samples at DSDP Site 215 show 61 Ma age oceanic crust (Von der Borch et al., 1974a), which corresponds to magnetic anomaly 27 following the geomagnetic polarity timescale of Cande and Kent (1995). This is in good agreement with anomalies 26 and 28-29 in the vicinity of the Site 215 (Figure 5b). Likewise the

248 oldest sediments at DSDP Site 213 are 57 Ma in age (Von der Borch et al., 1974b), which
249 corresponds well with anomalies 25 and 26 on either side of the site.

250

251 The magnetic pattern in the vicinity of the NER reveals that the age of the oceanic crust
252 to the west of the 86°E FZ increases towards the north from early Cenozoic to Late
253 Cretaceous, while the crust to the east of the 92°E FZ increases its age in both north and
254 south directions symmetric about the middle Eocene fossil Wharton Ridge segments.
255 Contrasting to these trends, the crust in between these FZ shows a complex age
256 succession with different age (65 and 42 Ma) fossil ridge segments (Figure 5). The ridge
257 segments abandoned at anomaly 30 and at anomaly 19 by ridge jumps are identified in
258 the equatorial region and in the area between 12° and 14°S latitudes, respectively.

259

260 **5. Tectonic Evolution of the Ninetyeast Ridge**

261

262 New $^{40}Ar/^{39}Ar$ ages of basaltic core samples from DSDP Sites 214, 216, 254 and ODP
263 Sites 756-758 show that the NER is age progressive for a distance of 3980 km, north to
264 south, spanning 77 to 43 Ma (Pringle et al., 2007, 2008). A plot of age versus latitude
265 displays remarkable linearity (Figure 6), with age decreasing to the south and a volcanic
266 propagation rate of 118±5 km/Myr (Pringle et al., 2008). This contrasts with earlier dates
267 that implied a significantly slower rate of 86±12 km/Myr (Duncan, 1978, 1991).
268 Comparison of the NER age progression with nearby magnetic anomalies indicates that
269 the NER lengthened much more rapidly than adjacent lithosphere (Figure 6). In regions
270 west of the 86°E FZ and east of the 90°E FZ, magnetic lineations 33 and 20,
271 corresponding to approximately to 77 and 43 Ma, respectively, are separated by ~2000

km (Figure 6a), revealing that the crust was created at a rate of ~58 km/Myr. In other regions closer to NER (between 86°E FZ and NER; between 89°E FZ and 90°E FZ), the oceanic crust was formed at comparable rates ranging from 48 to 55 km/Myr (Figure 6b). This discrepancy is a result of the difference between relative plate velocity, recorded by seafloor magnetic lineations, and the volcanic propagation rate of the NER, which reflects the velocity of the Indian plate relative to the hot spot.

The propagation rate of NER volcanism is about twice that of the half-spreading rates recorded on the Indian plate, or similar to the full-spreading rate between the Antarctic and Indian plates. The motion of the Antarctic plate relative to the hot spot reference frame at this time was slow (Acton, 1999; Besse and Courtillot, 2002). Thus, relative to a nearly fixed Antarctic plate, the Indian plate was moving northward at about the full spreading rate, and the Wharton spreading center itself was migrating northward at about the half spreading rate. It would thus seem that the NER volcanic propagation simply records this full spreading rate as postulated previously (e.g., Royer et al., 1991). Because of its rapid northward drift relative to the NER hot spot, the Wharton spreading ridge should have simply crossed over the hot spot, and subsequent volcanism would have occurred on the Antarctic plate. However, the eruption ages for the NER core samples are similar to the nearby magnetic anomalies indicating that the Wharton spreading ridge remained relatively close to the hot spot throughout much of the NER history (Figure 6). This circumstance required that some tectonic mechanism acted to keep the spreading ridge close to the hot spot; we argue that ridge jumps are that mechanism.

5.1 Wharton Ridge Segments and Kerguelen Hot spot Interactions

Using an updated magnetic data set, we present an improved interpretation of magnetic anomalies, particularly immediately to the east and west of the NER (Figures 5a and 5b), which supersedes earlier anomaly identifications in this region (Sclater and Fisher, 1974; Liu et al., 1983; Royer et al., 1991; Krishna et al., 1995). From the trends of the FZ and the NER, it is found that the 89°E FZ crosses the NER obliquely between 15°S and 10°S latitudes (Figures 5a and 5b). Consequently the NER was formed in two different spreading corridors of oceanic crust: the north part of the ridge active before ~62 Ma is situated between the 89°E FZ and the 90°E FZ, while the south part of the NER is located between the 86°E FZ and the 89°E FZ.

As described in Section 4, the oceanic crust between the 86°E and 90°E FZs shows non-monotonic sequences of magnetic lineations caused by ridge jumps, with two major jumps occurring at 65 and 42 Ma (Figures 5a and 5b). At ~90 Ma, the Indian plate was bounded on the southwest side by the Wharton and India-Antarctica ridges, which were connected through the 86°E transform fault (Krishna et al., 1995) and the Kerguelen hot spot was located beneath the Indian plate at a moderate distance from the Wharton Ridge segments. During the first spreading reorganization during the Late Cretaceous, a ridge segment immediately west of the NER ceased its activity at ~65 Ma and jumped southward to a place between the locations of magnetic anomalies 33 and 32n.2. This spreading segment also broke into three smaller sub-segments. The ridge jump created a fossil ridge segment, now located near the equator (Figure 5a), and transferred oceanic crust from the Antarctic plate formed between magnetic anomalies just younger than 30 to just older than 32n.2 to the Indian plate (Figures 5a, 7b). During

the second spreading jump at ~52 Ma, two sub-segments to the west of the NER jumped northward to crust formed between anomalies 25 and 26 (Figure 5b), and transferred oceanic crust from the Indian plate formed between magnetic anomalies just younger than 24n.2 to just older than 25 to the Antarctic plate (Figures 5b, 7d), while a third sub-segment closer to the NER appears to have jumped southward into pre-anomaly 34 oceanic crust. Finally, in the third spreading reorganization the entire Wharton Ridge system, including all three sub-segments, ceased spreading soon after middle Eocene anomaly 19. This process eventually led to unification of the Indian and Australian plates into a single Indo-Australian plate.

Considering the complex magnetic anomaly-derived age progression together with identified fossil ridge segments on both sides of the NER, the progression of ages determined from drill core samples (Figures 5 and 6), and proximity of the hot spot to spreading centers, we suggest two possible explanations for the ridge jumps with respect to the Kerguelen hot spot. With the observation of a few large ridge jumps to the west of the NER and the apparent continuity of the hot spot track, evolution of the NER may be explained by the positioning the Kerguelen hot spot beneath the Indian plate continuously from 77 to 43 Ma. This model requires a large amount of Antarctic plate lithosphere to be transferred to the Indian plate via spreading center jumps to the south away from the hot spot. Although this model appears to be simple because it allows the NER to form simply and with a monotonic age progression, the jumping of the ridge away from the hot spot appears counter to the widely-held idea that the excess heat and dynamic uplift over the hot spot weakens the lithosphere, causing the spreading center to jump toward the hot spot position. Observations on ridge-hot spot

interactions at other locations led several researchers (Brozena and White, 1990; Small, 1995; Hardarson et al., 1997; Mittelstaedt et al., 2011) to conclude that ridge segments jump repeatedly towards a hot spot, even when the overall motion of the ridge may be away from the hotspot. It is thought that warm upper mantle temperatures weaken the lithosphere and the hot spot-imposed stress field provides necessary conditions for rifting. A possible explanation for the unusual behavior of the ridge jumps near the NER is that regional stress changes caused these ridge jumps, overriding local stresses caused by the hot spot.

An alternative model, which fits the notion of the spreading ridge jumping toward the hot spot, has the Wharton Ridge system drifting northward of the hot spot and the ridge segment beneath the NER repeatedly jumping back to the hot spot location, thereby accreting bits of the NER from the Antarctic plate to the Indian plate. NER components formed on the Antarctic plate should have reverse age progressions (i.e., become younger towards the north). The existing, reliable age data (Figure 6) are sparse, but remarkably consistent with a simple, linear age progression. Thus, if this explanation is true, reverse age segments must occur in the gaps between dated samples or the ridge jumps were frequent and small enough that the reversed age trends are not resolvable (Sager et al., 2010). Although it requires the added complexity of additional ridge jumps, we prefer this hypothesis because it allows the ridge segment to jump to the hot spot and it fits the observed hot spot-ridge offsets interpreted from magnetic lineations, which show the hot spot to the south of the Wharton Ridge during the Cenozoic (Figure 7).

368 Various stages of possible interactions between the spreading center and the Kerguelen
369 hot spot during the formation of the NER are presented in Figure 8. Initially the hot
370 spot was beneath the Indian plate and possibly at some distance from the spreading
371 center, resulting in intraplate volcanism on the Indian plate now in the Bay of Bengal
372 region (Figure 8a). This postulation is supported by the presence of regional
373 lithospheric flexure determined beneath the NER in the Bay of Bengal region (Gopala
374 Rao et al., 1997; Tiwari et al., 2003; Krishna et al., 2009b). Subsequently, rapid
375 northward migration of the Wharton spreading ridge allowed it to coincide with the hot
376 spot for on-axis volcanism (Figure 8b), which may have emplaced sections of NER
377 simultaneously on both plates (with much of that formed on the Antarctic plate
378 eventually captured via ridge jumps). Evidence of Kerguelen hot spot volcanism on the
379 Antarctic plate during the formation of the NER is basalts from Skiff Bank (Kerguelen
380 Plateau) dated at 68 Ma (Coffin et al., 2002).
381
382 Further spreading center migration would have placed the hot spot beneath the
383 Antarctic plate for near ridge or ridge-flank volcanism (Figure 8c). With continued
384 ridge migration, the hot spot moved farther from the spreading ridge beneath the
385 Antarctic plate. The stress field created by the hot spot may have caused uplift and
386 weakening of the overlying oceanic lithosphere, resulting in the initiation of rifting and
387 spreading within the Antarctic plate and leading to southward ridge jumps. It is possible
388 that hot spot material flowed along the base of the lithosphere to reach the spreading
389 center for on-axis volcanism (Figure 8d), even when the hot spot was not located in the
390 vicinity of the spreading ridge crest. This mechanism has been called upon to explain
391 some features of the Amsterdam-St. Paul plateau, which is nearby and had a similar

history of construction (Maia et al., 2011). In addition, the magnetic anomalies suggest that the NER formed within a relatively narrow spreading center corridor with long-offset FZ segments (Figure 7), and some NER volcanism may have occurred along the FZ or the long-offsets may have encouraged small bits to break off of the Antarctic plate (i.e., microplates or ridge jumps). The continuous process of hot spot-spreading ridge interaction may have provided necessary conditions to cause multiple ridge jumps. This behavior is also consistent with models of ridge-hot spot interaction in which ridge jumps are promoted by hot spot heating of the lithosphere and perturbations of the local stress field, and form preferentially in younger lithosphere in systems with relatively fast plate velocity (Mittelstaedt et al., 2008, 2011).

5.2 Evolution of Extra Length of the NER with respect to Simple Plate Drift

It is obvious from age data of the NER and adjacent oceanic crust evolved within the same time-frame (77 to 43 Ma) that the length of the NER is much greater than the stretch of the oceanic crust evolved on the Indian plate (Figure 6). The NER emplacement rate was almost a factor-of-two faster than the rate of accretion of oceanic crust. The extra length of the NER track is ~2000 km, and because the Wharton spreading ridge would have quickly passed the hot spot, it is necessary to postulate other explanations than simple plate drift. Furthermore, the linear trend of NER ages (Pringle et al., 2008) implies that significant slowing of the Indian plate, considered as a response of the continental collision between India and Asia, did not start until completion of construction of the entire NER (~42 Ma). Slow-spreading rates (2.4-2.9 cm/yr) observed in the present study (Figures 4b and 4c), particularly in two phases (anomalies 31 to 30 and again from 21 to 19) appear to indicate waning stages of ridge

segments in the process of abandonment, but not a response to the slowing of the Indian plate motion.

As discussed in the previous section, the Kerguelen hot spot was initially in an off-ridge position during the formation of the NER in the Bay of Bengal region (Figure 8a), therefore the Wharton spreading ridge may have taken considerable time to reach the position of the hot spot and to move away to the north. In the process, the northern part of the NER, at least down to 5°N latitude, was created by two different plate motions, viz., by plate motion relative to the hot spot and by a plate boundary (Wharton spreading ridge) migration. The latter activity may have added some additional length of volcanic constructs to the NER track. During the emplacement of the central part of the NER, particularly from 5°N to 11°S latitudes, the hot spot and ridge segments were often in close proximity and this may have allowed the hot spot to form components of the NER on the Antarctic plate that were subsequently transferred to the Indian plate through southward ridge jumps (Figure 7b-d).

A critical question for NER evolution is how many such ridge jumps occurred. Our interpretation of the magnetic data set in basins adjacent to the NER is a small number of larger ridge jumps. However, both Krishna et al. (1999) and Desa et al. (2009) have mapped smaller southward ridge jumps near the NER at ~76 and 54 Ma, respectively. Sager et al. (2010) concluded, based on identification of extensive faulting within the NER structure, that numerous small-scale ridge jumps may have occurred and that the hot spot and Wharton spreading ridge may have remained in close proximity. Small ridge jumps are an attractive solution to the paradox that large ridge jumps would result

440 in long segments of reversed age trend yet existing age data are remarkably linear
441 (Figure 6). Such ridge jumps may also explain the apparent increased FZ offsets during
442 the Cenozoic on the Wharton Ridge near NER (Figure 7).
443
444 Although it is true that existing NER age data are sparse and might not detect a
445 reversed age segment, the deviant segment would have to hiding in the gaps of the
446 current data. Further, magnetic anomalies near the NER are very difficult to interpret
447 (Figure 3) presumably because the extended history of hot spot and spreading center
448 volcanism does not result in simple magnetization of the ocean crust and discernable
449 patterns of magnetic anomalies. Another factor is that small ridge jumps can be difficult
450 to detect because this requires the recognition of a repeated anomaly pattern that may
451 not be clear unless there are several mirrored anomalies (i.e., a seafloor spreading for a
452 significant time). Thus, despite the improvement with the current magnetic dataset over
453 prior compilations, it is not surprising that small ridge jumps are not recognized in the
454 pattern of magnetic anomalies along the NER. More detailed magnetic surveys with
455 closely spaced data would be needed to recognize of small jumps, as shown, for
456 example, at Amsterdam-St. Paul Plateau (Maia et al., 2011).
457
458 Besides the processes discussed above, absolute hot spot movement also may have
459 contributed to the lengthening of the NER. Paleomagnetic analyses and mantle flow
460 models have been used to infer 7-10° (800-1100 km) of southward motion of the
461 Kerguelen hot spot during the past 120 Myr (Klootwijk et al., 1991; Antretter et al.,
462 2002; O'Neill et al., 2003). Such southward motion would also lengthen the NER, but

463 we cannot quantify the north-south hot spot motion because our data set only shows the
464 relative motions of the hot spot and spreading center.
465
466 **6. Summary and conclusions**
467
468 An investigation of magnetic anomaly profiles and other geophysical data around the
469 NER and adjacent Central Indian and Wharton basins together with newly determined
470 radiometric ages from igneous rocks cored at DSDP and ODP Sites on the NER has
471 provided new insights on the evolution of the NER and interactions between the
472 Wharton spreading ridge segments and the Kerguelen hot spot. Important observations
473 are as follows.
474
475 1. Magnetic anomaly studies of both the Central Indian and Wharton basins have
476 provided locations of magnetic lineations from 19 through 34 and fossil ridge
477 segments which ceased spreading at 65 and 42 Ma. The lineation offsets are further
478 constrained by narrow, linear gravity anomalies within satellite-derived gravity data
479 that we interpret as fracture zone features. The NER trends ~N 10°E and obliquely
480 crosses ~N 5°E oriented fracture zones. Thus in the south, the 89°E FZ borders the
481 NER on the east side, whereas in the north the same fracture zone borders the ridge
482 on the west side. In the central part between 11°S and 18°S, the fracture zone
483 obliquely crosses the NER.

484 2. The age of oceanic crust to the west of the 86°E FZ (Central Indian Basin) increases
485 towards the north from early Cenozoic to Late Cretaceous, while the crust to the
486 east of the 90°E FZ (Wharton Basin) increases its age in both the north and south
487 directions about 42 Ma fossil Wharton Ridge segments. Contrasting to these

patterns, the crust between the FZs near the NER shows a complex age succession together with fossil ridge segments of different ages (65 and 42 Ma).

3. Comparison of ages of oceanic crust, directly to the east and west of the NER with newly determined radiometric ages at DSDP Sites 216, 214, 254 and ODP Sites 756-758 shows that the NER lengthened at a rate twice that of adjacent oceanic crust.

4. The resulting difference in lengths of the NER (~3980 km) and adjacent oceanic crust (~2000 km) constructed from 77 to 43 Ma is remarkable and requires a geodynamical explanation. During the formation of the NER, the distance between the Kerguelen hot spot and spreading ridge segments changed due to the northward migration of the Wharton spreading ridge, southward ridge jumps, and possibly southward motion of the hot spot. Spreading ridge migration probably resulted in the Kerguelen hot spot underlying the Antarctic plate during the early Cenozoic, and led to formation of volcanic edifices on the Antarctic plate by ridge-flank volcanism and by lateral transport of hot spot melt along the ridge-axis. The southward ridge jumps transferred parts of the NER originally formed on the Antarctic plate to the Indian plate and were the major the major contribution to the extra lengthening of the NER.

Acknowledgments

We are indebted to captain, ship crew, and technicians of the R/V *Roger Revelle* for their efforts during the international scientific expedition (KNOX06RR) of the Ninetyeast Ridge. The field program was supported by the National Science

512 Foundation Grants OCE-0550743 and OCE-05499852. Honey Abraham is thankful to
513 CSIR, New Delhi, for the support of student research fellowship (NET-JRF). DGR is
514 thankful to DST, New Delhi for supporting his research activities through DST-RFBR
515 project 1103. We thank Jon Bull, Chuck DeMets and anonymous Associate Editor for
516 their critical comments and suggestions on the manuscript, with which the manuscript
517 has improved greatly. This is NIO contribution number xxxx.

518 **References:**

519 Acton, G. D., (1999), Apparent polar wander of India since the Cretaceous with
520 implications for regional tectonics and true polar wander, *Mem. Geol. Soc. India*,
521 44, 129-175.

522 Antretter, M., B. Steinberger, F. Heider, and H. Soffel (2002), Paleolatitudes of the
523 Kerguelen hot spot: new plaeomagnetic results and dynamic modeling, *Earth*
524 *Planet. Sci. Lett.*, 203, 635-650.

525 Besse, J., and V. Courtillot (2002), Apparent and true polar wander and the geometry of
526 the geomagnetic field over the last 200 Myr, *J. Geophys. Res.*, 107(B11), 2300,
527 doi:10.1029/2000JB000050,.

528
529 Brozena, J. M., and R. White (1990), Ridge jumps and propagations in the South
530 Atlantic Ocean, *Nature*, 348, 149–152, doi:10.1038/348149a0.

531 Bull, J. M. (1990), Structural style of intraplate deformation, Central Indian Ocean
532 Basin: evidence for the role of fracture zones, *Tectonophysics*, 184, 213-228.

533 Bull J. M., C. DeMets, K. S. Krishna, D. J. Sanderson, and S. Merkouriev (2010),
534 Reconciling plate kinematic and seismic estimates of lithospheric convergence in
535 the central Indian Ocean, *Geology*, 38, 307-310.

536 Cande, S. C., and D. V. Kent (1995), Revised calibration of the geomagnetic polarity
537 time scale for the late Cretaceous and Cenozoic, *J. Geophys. Res.*, 100, 6093-6095.

538 Chamot-Rooke, N., F. Jestin, B. de Voogd, and Phedre Working Group (1993),
539 Intraplate shortening in the central Indian Ocean determined from a 2100-km-long
540 north-south deep seismic reflection profile, *Geology*, 21, 1043-1046.

541 Coffin, M. F., M. S. Pringle, R. A. Duncan, T. P. Gladczenko, M. Storey, R. D. Müller,
542 and L. A. Gahagan (2002), Kerguelen hot spot magma output since 130 Ma, *J.*
543 *Petrology*, 43, 1121-1139.

544 Curray, J. R., F. J. Emmel, D. G. Moore, and W. R. Russel (1982), Structure, tectonics,
545 and geological history of the northeastern Indian Ocean, in The Ocean Basins and
546 Margins, vol. 6, *The Indian Ocean*, A. E. Nairn and F. G. Stheli (eds.), pp. 399–
547 450, Plenum, New York.

548 Delescluse, M., and N. Chamot-Rooke (2007), Instantaneous deformation and
549 kinematics of the India-Australia plate, *Geophys. J. Int.*, 168, 818–842.

550 Deplus, C., M. Diament, H. Hebert, G. Bertrand, S. Dominguez, J. Dubois, J. Malod, P.
551 Patriat, B. Pontoise, and J.J. Sibilla (1998), Direct evidence of active deformation in
552 the eastern Indian oceanic plate, *Geology*, 26, 131-134.
553
554 Desa, M., M. V. Ramana, and T. Ramprasad (2009), Evolution of the Late Cretaceous
555 crust in the equatorial region of the Northern Indian Ocean and its implication
556 in understanding the plate kinematics, *Geophys. J. Int.,* 177, 1265–1278.
557
558 Duncan, R. A. (1978), Geochronology of basalts from the Ninetyeast Ridge and
559 continental dispersion in the eastern Indian Ocean, *J. Volc. Geotherm. Res.*, 4, 283-
560 305.
561

562 Duncan, R.A. (1991), Age distribution of volcanism along aseismic ridges in the
563 eastern Indian Ocean, *Proc. ODP, Sci. Res.*, 121 507-517.
564
565 Fisher R. L., M. J. Jantsch, and R. L. Comer (1982), General Bathymetric chart of the
566 Oceans (GEBCO); Canadian Hydrographic Service, Ottawa, Canada.
567
568 Gopala Rao, D., K. S. Krishna, and D. Sar (1997), Crustal evolution and sedimentation
569 history of the Bay of Bengal since the Cretaceous, *J. Geophys. Res.*, 102, 17,747–
570 17,768, doi:10.1029/96JB01339.

571 Gordon, R. G., C. DeMetes, and J.-Y. Royer (1998), Evidence for long-term diffuse
572 deformation of the lithosphere of the equatorial Indian Ocean, *Nature*, 395, 370-
573 374.

574 Hardarson, B. S., J. G. Fitton, R. M. Ellam, and M. S. Pringle (1997), Rift relocation - a
575 geochemical and geochronological investigation of a paleorift in northwest Iceland,
576 *Earth Planet. Sci. Lett.,* 153, 181–196, doi:10.1016/S0012-821X(97)00145-3.
577
578 Klootwijk, C. T., S. G. Jeff, J. W. Peirce, and G. M. Smith (1991), Constraints on the
579 Indian-Asia convergence: Paleomagnetic results from Ninetyeast Ridge, in: J. K.
580 Weissel, J. W. Pierce, E. Taylor and J. Alt (Eds.), *Proc. ODP, Sci. Results*, 121,
581 777-882.

582 Krishna, K. S., D. Gopala Rao, M. V. Ramana, V. Subrahmanyam, K. V. L. N. S.
583 Sarma, A. I. Pilipenko, V. S. Shcherbakov, and I. V. Radhakrishna Murthy (1995),
584 Tectonic model for the evolution of oceanic crust in the northeastern Indian Ocean

585 from the Late Cretaceous to the early Tertiary, *J. Geophys. Res.*, 100, 20,011–
586 20,024, doi:10.1029/94JB02464.

587 Krishna, K. S., M. V. Ramana, D. Gopala Rao, K. S. R. Murthy, M. M. Malleswara
588 Rao, V. Subrahmanyam, and K. V. L. N. S. Sarma (1998), Periodic deformation of
589 oceanic crust in the central Indian Ocean, *J. Geophys. Res.*, 103, 17,859–17,875,
590 doi:10.1029/98JB00078.

591 Krishna, K. S., D. Gopala Rao, L. V. Subba Raju, A. K. Chaubey, V. S. Shcherbakov,
592 A. I. Pilipenko, and I. V. Radhakrishna Murthy (1999), Paleocene on-axis hot spot
593 volcanism along the Ninetyeast Ridge: An interaction between the Kerguelen hot
594 spot and the Wharton spreading center, *Proc. Indian Acad. Sci. (Earth Planet. Sci.),*
595 108, 255–267.

596 Krishna, K. S., and D. Gopala Rao (2000), Abandoned Paleocene spreading center in
597 the northeastern Indian Ocean: Evidence from magnetic and seismic reflection data,
598 *Mar. Geol.*, 162, 215–224, doi:10.1016/S0025-3227(99)00085-7.

599 Krishna, K.S., Y.P. Neprochnov, D. Gopala Rao, and B. N. Grinko (2001a), Crustal
600 structure and tectonics of the Ninetyeast Ridge from seismic and gravity studies,
601 *Tectonics*, 20, 416 – 433, doi:10.1029/2001TC900004.

602 Krishna, K. S., J. M. Bull, and R. A. Scrutton (2001b), Evidence for multiphase folding
603 of the central Indian Ocean lithosphere, *Geology*, 29, 715–718, doi:10.1130/0091-
604 7613(2001).

605 Krishna, K. S., J. M. Bull, and R. A. Scrutton (2009a), Early (pre-8 Ma) fault activity
606 and temporal strain distribution in the central Indian Ocean, *Geology*, 37, 227–230.

607 Krishna K. S., L. Michael, R. Bhattacharyya, and T. J. Majumdar (2009b), Geoid and
608 gravity anomaly data of conjugate regions of Bay of Bengal and Enderby Basin -
609 new constraints on breakup and early spreading history between India and
610 Antarctica, *J. Geophys. Res.*, 114, B03102, doi:10.1029/2008JB005808.
611 Liu, C. S., J. R. Curray, and J. M. McDonald (1983), New constraints on the tectonic
612 evolution of the Eastern Indian Ocean, *Earth Planet. Sci. Lett.*, 65, 331-342.
613
614 Maia, M., I. Pessanha, E. Courreges, M. Patriat, P. Gente, C. Hémond, M. Janin, K.
615 Johnson, W. Roest, J-Y. Royer, and J. Vetteville (2011), Building of the
616 Amtersdam-St. Paul plateau: A 10 Myr history of a ridge-hot spot interaction and
617 variations in the strength of the hot spot source, *J. Geophys. Res.,* 116, B09104,
618 doi:10.1029/2010JB007768.
619
620 Mendel, V., M. Munschy, and D. Sauter (2005), MODMAG, a MATLAB program to
621 model marine magnetic anomalies, *Comput. & Geosci.,* 589–597.
622
623 Michael, L., and K. S. Krishna (2011), Dating of the 85°E Ridge (northeastern Indian
624 Ocean) using marine magnetic anomalies, *Curr. Sci.*, 100, 1314-1322.
625
626 Mittelstaedt, E., G. Ito, and M. D. Behn (2008), Mid-ocean ridge jumps associated with
627 hot spot magmatism, *Earth Planet. Sci. Lett.*, 266, 256-270.
628
629 Mittelstaedt, E., G. Ito, and J. van Humen (2011), Repeat ridge jumps associated with
630 plume-ridge interaction, and ridge migration, *J. Geophys. Res.*, 116, B01102,
631 doi:10.1029/2010JB007504.

632 O'Neill, C., D. Müller, and B. Steinberger (2003), Geodynamic implications of moving
633 Indian Ocean hot spots, *Earth Planet. Sci. Lett.*, 215, 151-168.
634
635 Patriat, P., and J. Segoufin (1988), Reconstruction of the central Indian Ocean,
636 *Tectonophysics*, 155, 211-234.
637
638 Peirce, J. W. (1978), The northward motion of India since the late Cretaceous,
639 *Geophys. J. Royal Astro. Soc. J.*, 52, 277-311.
640
641 Peirce, J. W., J. K. Weissel et al., (1989), *Proc. ODP, Init. Repts.*, 121, pp.1000.
642
643 Pilipenko, A. I. (1996), Fracture zones of the Ninetyeast Ridge area, Indian Ocean,
644 *Geotectonics*, 30, 441-451.
645
646 Pringle, M. S., F. A. Frey, E. M. Mervine, and W. W. Sager (2007), New Ar/Ar ages
647 from the Ninetyeast Ridge, Indian Ocean: Beginning of a robust Indo-Atlantic hot
648 spot reference frame, *EOS, Trans. AGU, 88* (52), Fall Mtg. Supplement, abstract
649 U13A-0871.
650
651 Pringle, M. S., F. A. Frey, and E. M. Mervine (2008), A simple linear age progression
652 for the Ninetyeast Ridge, Indian Ocean: New constraints on Indian plate motion and
653 hot spot dynamics, *EOS, Trans. AGU, 89* (53) Fall Mtg. Suppl., abstract T54B-03.
654
655 Royer, J.-Y., and D. T. Sandwell (1989), Evolution of the eastern Indian Ocean since
656 the late Cretaceous: Constraints from Geosat altimetry, *J. Geophys. Res.*, 94,
657 13,755–13,782, doi:10.1029/JB094iB10p13755.
658

659 Royer, J.-Y., J. W. Peirce, and J. K. Weissel (1991), Tectonic constraints on the hot-
660 spot formation of Ninetyeast Ridge, *Proc. ODP, Sci. Res.*, 121, 763-776.

661 Royer, J.-Y., and R.G. Gordon (1997), The motion and boundary between the
662 Capricorn and Australian plates, *Science*, 277, 1268 – 1274,
663 doi:10.1126/science.277.5330.1268.
664
665 Sandwell, D. T., and W. H. F. Smith (1997), Marine gravity from Geosat and ERS-1
666 satellite altimetry, *J. Geophys. Res.*, 102, 10039-10054.

667 Sclater, J. G., and R. L. Fisher (1974), Evolution of the east central Indian Ocean, with
668 emphasis on the tectonic setting of the Ninetyeast Ridge, *Geol. Soc. Am. Bull.*, 85**,**
669 683-702.

670 Sager, W.W. et al., (2007), Cruise Report KNOX06RR R/V Roger Revelle, pp. 1-82.
671 (http://earthref.org/erda/1172).

672 Sager, W. W., C. F. Paul, K. S. Krishna, M. Pringle, A. E. Eisin, F. A. Frey, D. Gopala
673 Rao, and O. Levchenko (2010), Large fault fabric of the Ninetyeast Ridge implies
674 near-spreading ridge formation, *Geophys. Res. Lett.*, 37, L17304, doi:10.1029/
675 2010GL044347.

676 Small, C. (1995), Observation of ridge–hot spot interactions in the Southern Ocean, *J.*
677 *Geophys. Res.*, 100, 17931–17946.

678 Subrahmanyam, C., R. Gireesh, S. Chand, K. A. Kamesh Raju, and D. Gopala Rao
679 (2008), Geophysical characteristics of the Ninetyeast Ridge – Andaman island arc/
680 trench convergent zone, *Earth Planet. Sci. Lett.*, 266, 29-45.

681 Tiwari, V. M., M. Diament, and S. C. Singh (2003), Analysis of satellite gravity and
682 bathymetry data over Ninety-East Ridge: variation in the compensation mechanism
683 and implication for emplacement process, *J. Geophys. Res.*, 108(B2), 2109,
684 doi:10.1029/ 2000JB000047.

685 Von der Borch, C. C., J. G. Sclater et al., (1974a), Site 215*, Init. Repts. DSDP,* 22, 193-
686 211.

687 Von der Borch, C. C., J. G. Sclater et al., (1974b), Site 213, *Init. Repts. DSDP*, 22, 193-
688 211.

689 Weissel, J. K., R. N. Anderson, and C. A. Geller (1980), Deformation of the Indo-
690 Australian plate, *Nature*, 287, 284-291.

691 **Figure Captions:**

692 Figure 1: General bathymetry of the Indian Ocean showing mid-oceanic ridge systems,
693 oceanic basins, aseismic ridges and plateaus. Numbered solid triangles and
694 circles show DSDP and ODP sites, respectively, that are mentioned in the
695 text. BR = Broken Ridge, CR = Carlsberg Ridge, CIR = Central Indian
696 Ridge, SWIR = Southwest Indian Ridge, SEIR = Southeast Indian Ridge.

697 Figure 2: Magnetic tracks in the vicinity of the NER. Red solid-lines indicate magnetic
698 profiles acquired from different data sources (KNOX06RR cruise, NGDC,
699 NIO and TIOG databases; the key of profile identifiers with specific cruises
700 is given in Table 1), which are analyzed in the present study. Detailed
701 geophysical data including multibeam bathymetry, 10-fold multichannel
702 seismic reflection, and magnetic profiles were acquired in locations
703 represented by yellow-colored rectangles on top of the NER. Solid triangles
704 and circles indicate DSDP and ODP drill sites, respectively.

705 Figure 3: Magnetic anomaly profiles shown on top of the satellite free-air gravity image
706 of the northeastern Indian Ocean (prepared from database of Sandwell and
707 Smith, 1997). The map is divided into two parts for better visualization.

708 (a) Magnetic anomaly data are plotted along the ship tracks. White dashed
709 lines are drawn to follow narrow gravity features that define oceanic
710 fracture zones. DSDP and ODP sites are shown by solid red triangles and
711 solid black circles, respectively. Ages indicated at each drill site are from
712 the geochronology data published by Pringle et al. (2008).

713 (b) Southern part of the satellite gravity and magnetic anomaly profile data
714 of the northeastern Indian Ocean.

715 Figure 4: Observed magnetic anomaly profile data are correlated with synthetic
716 magnetic profiles.
717 (a) West of the 86°E FZ. Spreading-type magnetic anomalies 21 through 34
718 are identified and correlated from profile to profile. The geomagnetic
719 polarity time scale of Cande and Kent (1995) was used for assigning the
720 age to the magnetic lineations.
721 (b) East of the NER. Magnetic anomalies 20 through 34 and fossil ridge
722 segments (of middle Eocene age) are identified. The offsets in magnetic
723 lineations are used to define several fracture zones. Hashed lines ("FRS")
724 denote abandoned ("fossil") spreading centers
725 (c) Between the 86°E FZ and the NER. Magnetic anomalies 21 through 34
726 are identified and fossil ridge segments (FRS) of latest Cretaceous and
727 middle Eocene age are identified. The magnetic lineations identified
728 between the FRS have lost systematic continuity in anomaly sequence
729 due to ridge jumps.

730 Figure 5: Interpreted magnetic lineations (black lines), fossil ridge segments (solid
731 stippled line) and oceanic fracture zones (dashed lines) of the northeastern
732 Indian Ocean. Magnetic lineations indicated with blue lines are adopted from
733 earlier studies (Royer et al., 1991; Krishna and Gopala Rao, 2000). The
734 tectonic map is divided into two parts for better visualization. Magnetic
735 profiles are shown particularly to support the anomaly identifications,
736 correlations and offsets. Fracture zones are tightly constrained by satellite

737 gravity data. Bathymetric contour 3000 m and less water depths are shaded
738 for outlining the physiography of the NER and other features. (a) northern
739 NER; (b) southern NER.

740 Figure 6: Comparison of rates of ocean crust creation in different spreading corridors
741 and the volcanic propagation rate on the NER. (a) Seafloor created in the
742 Central Indian and Wharton basins, west of the 86ºE and east of the 92ºE
743 fracture zones, respectively. (b) Radiometric ages from DSDP and ODP sites
744 along the NER, seafloor created immediately to the west between the 88ºE
745 and 89ºE fractures zones, and seafloor created immediately to the east
746 between the 89ºE and 90ºE fracture zones. Black solid-dots show ages of
747 drill core samples (Pringle et al, 2008); open symbols denote seafloor
748 spreading magnetic anomalies (Figure 4 & 5). FRS indicates fossil ridge
749 segment. Note the northward spreading center jump in the seafloor between
750 the 86ºE and 88ºE fracture zones after C24n.2 time into C25 age crust, and
751 subsequent spreading up to the FRS just after C20.

752 Figure 7: Tectonic evolution of the NER with respect to adjacent spreading ridge
753 segments for four different ages from the late Cretaceous to early Cenozoic.
754 Solid line shows the relatively well-constrained location of the Wharton
755 spreading centers and transform faults on either side of the NER. Dashed line
756 represents the Wharton spreading segment active directly under the NER at
757 that time; its location is only approximate because the complex volcanic
758 history of the crust directly under the NER did not allow the formation of
759 discernable magnetic anomaly patterns. Two episodes of spreading center
760 jumps and transferred crust can be specifically identified directly to the west

761 of the NER. The more frequent, smaller spreading center jumps proposed for
762 the corridor directly under the NER cannot be specifically identified, but
763 those corridors should include about 50% crust transferred from the Antarctic
764 (ANT) to Indian (IND) plates.

765 Figure 8: Sketch model showing possible interactions between the Kerguelen hot spot,
766 proximal ridge segments and oceanic lithosphere during the formation of the
767 NER. The model is developed based on the conceptual model of Mittelstaedt
768 et al. (2011) and the results obtained from the present study. (a) Off-axis
769 volcanism when the hot spot was located north of the spreading ridge
770 segments; (b) On-axis volcanism when the hot spot was located at the
771 spreading ridge after northward migration of the plate boundary (Wharton
772 Ridge) with respect to a nearly fixed Antarctic plate; (c) Volcanism on the
773 ridge flank when the hot spot was located beneath the weak lithosphere of the
774 Antarctic plate; and (d) On-axis melt flow when the hot spot was located off-
775 axis beneath older-age lithosphere of the Antarctic plate.

776 Table 1: Details of profiles ids and data bases used in the present study

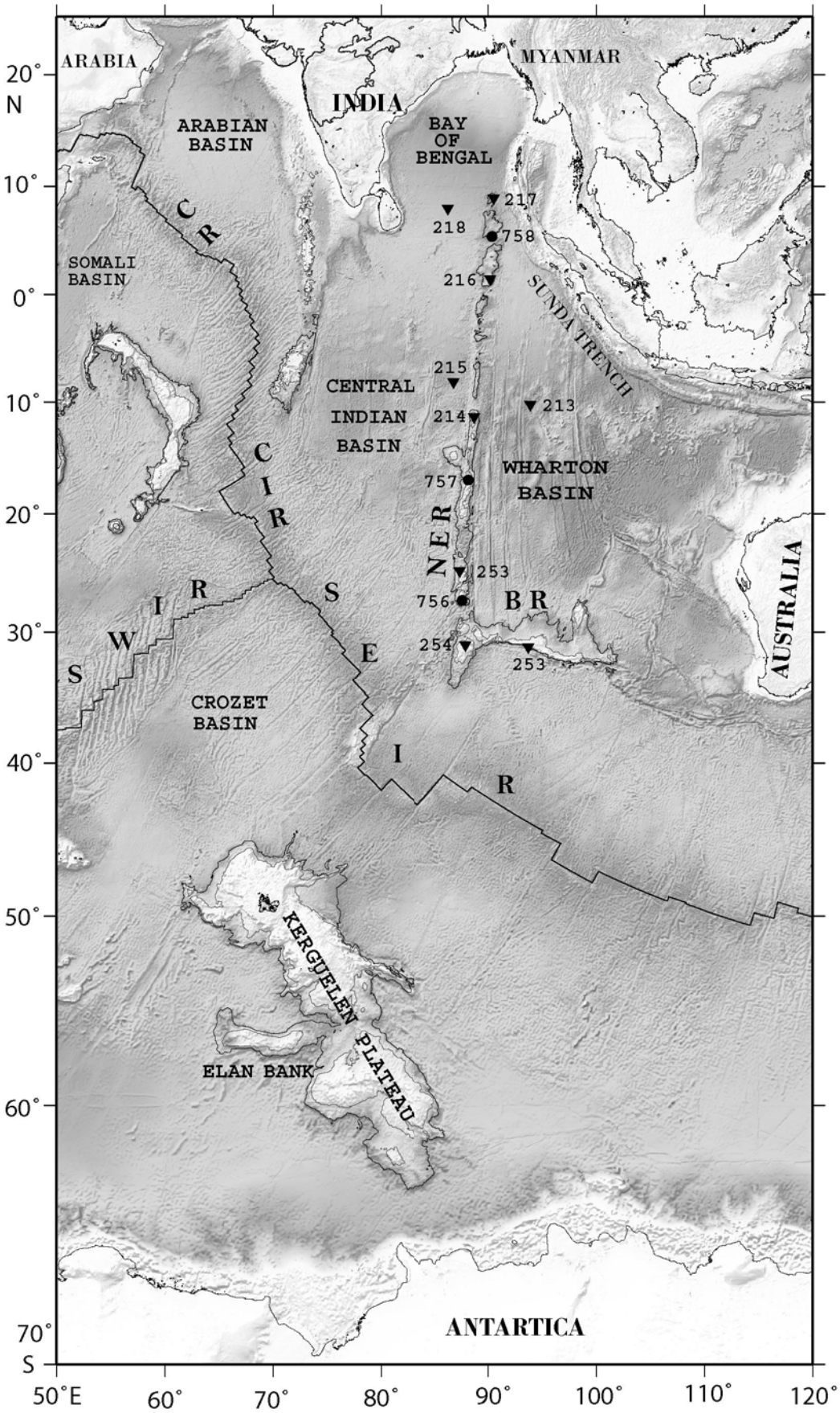
ARABIA
INDIA
MYANMAR
ARABIAN BASIN
BAY OF BENGAL
SOMALI BASIN
CENTRAL INDIAN BASIN
WHARTON BASIN
SUNDA TRENCH
AUSTRALIA
CROZET BASIN
KERGUELEN PLATEAU
ELAN BANK
ANTARTICA
CRISP
SWIR
NERBR
217
218
758
216
215
213
214
757
253
756
254
253
20° N
10°
0°
10°
20°
30°
40°
50°
60°
70° S
50°E
60°
70°
80°
90°
100°
110°
120°

Figure 1

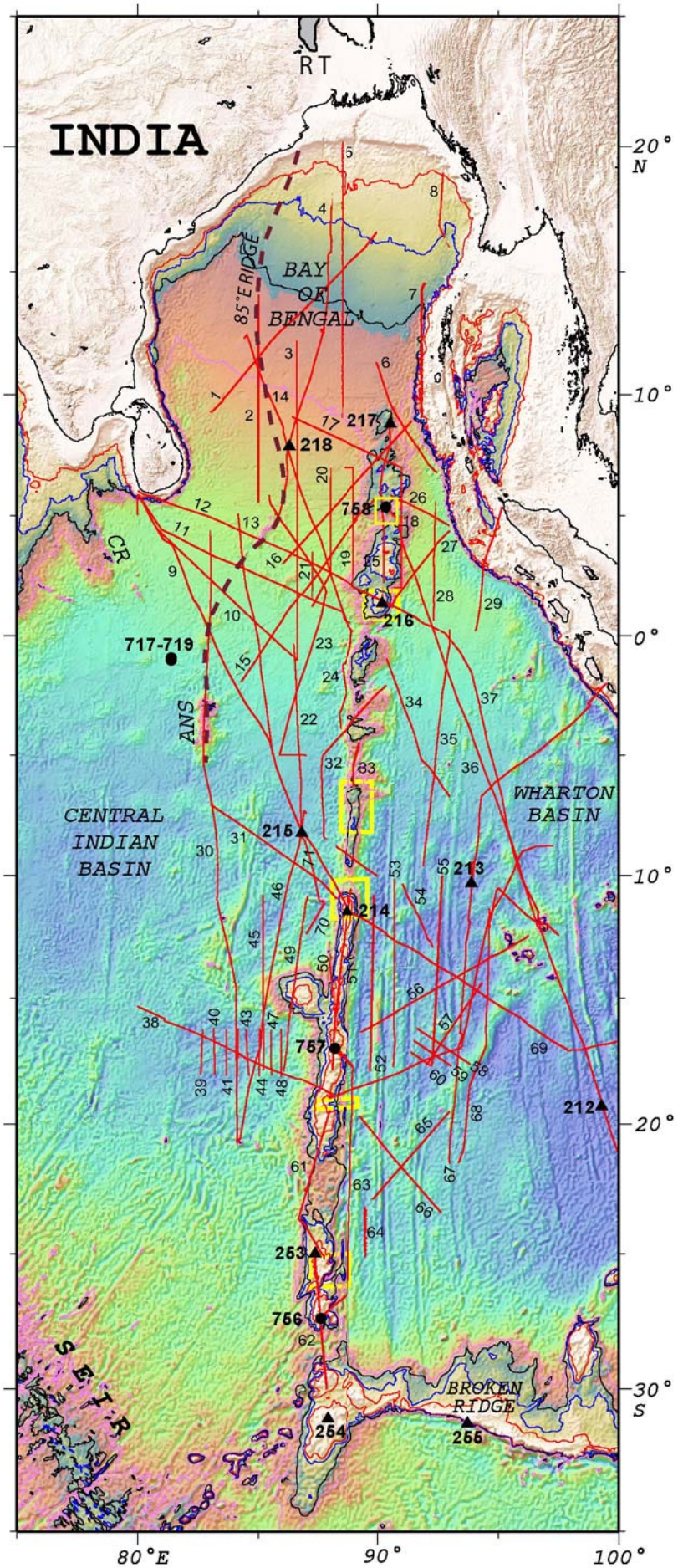
INDIA
RT
BAY OF BENGAL
85°E RIDGE
CR
ANS
CENTRAL INDIAN BASIN
WHARTON BASIN
BROKEN RIDGE
SEIR
217
218
758
216
717-719
215
214
213
757
212
253
756
254
255
20° N
10°
0°
10°
20°
30° S
80°E
90°
100°

Figure 2

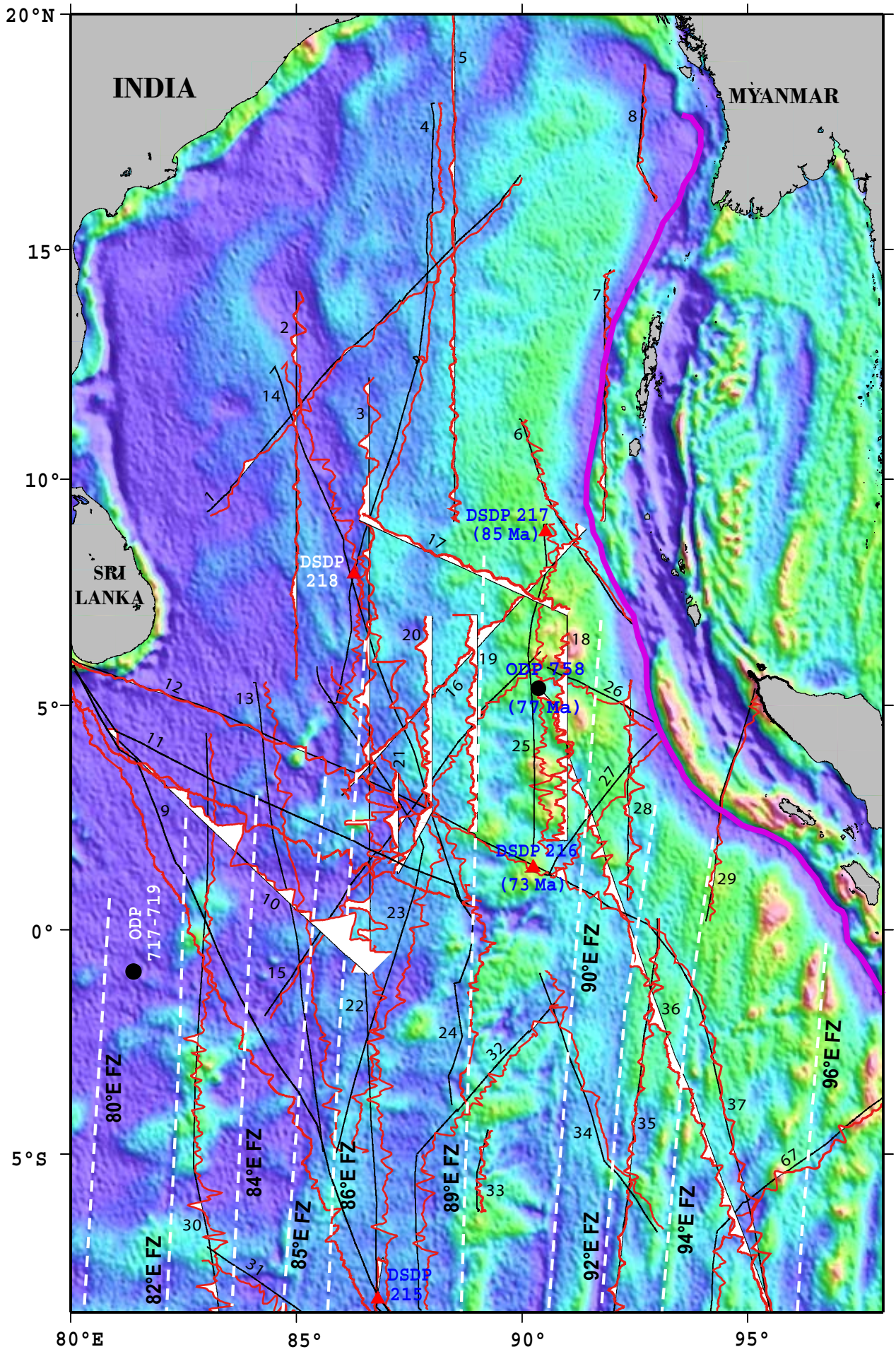
INDIA
MYANMAR
SRI LANKA
DSDP 218
DSDP 217 (85 Ma)
ODP 758 (77 Ma)
DSDP 216 (73 Ma)
ODP 717-719
DSDP 215
80°E FZ
82°E FZ
84°E FZ
85°E FZ
86°E FZ
89°E FZ
90°E FZ
92°E FZ
94°E FZ
96°E FZ
20°N
15°
10°
5°
0°
5°S
80°E
85°
90°
95°

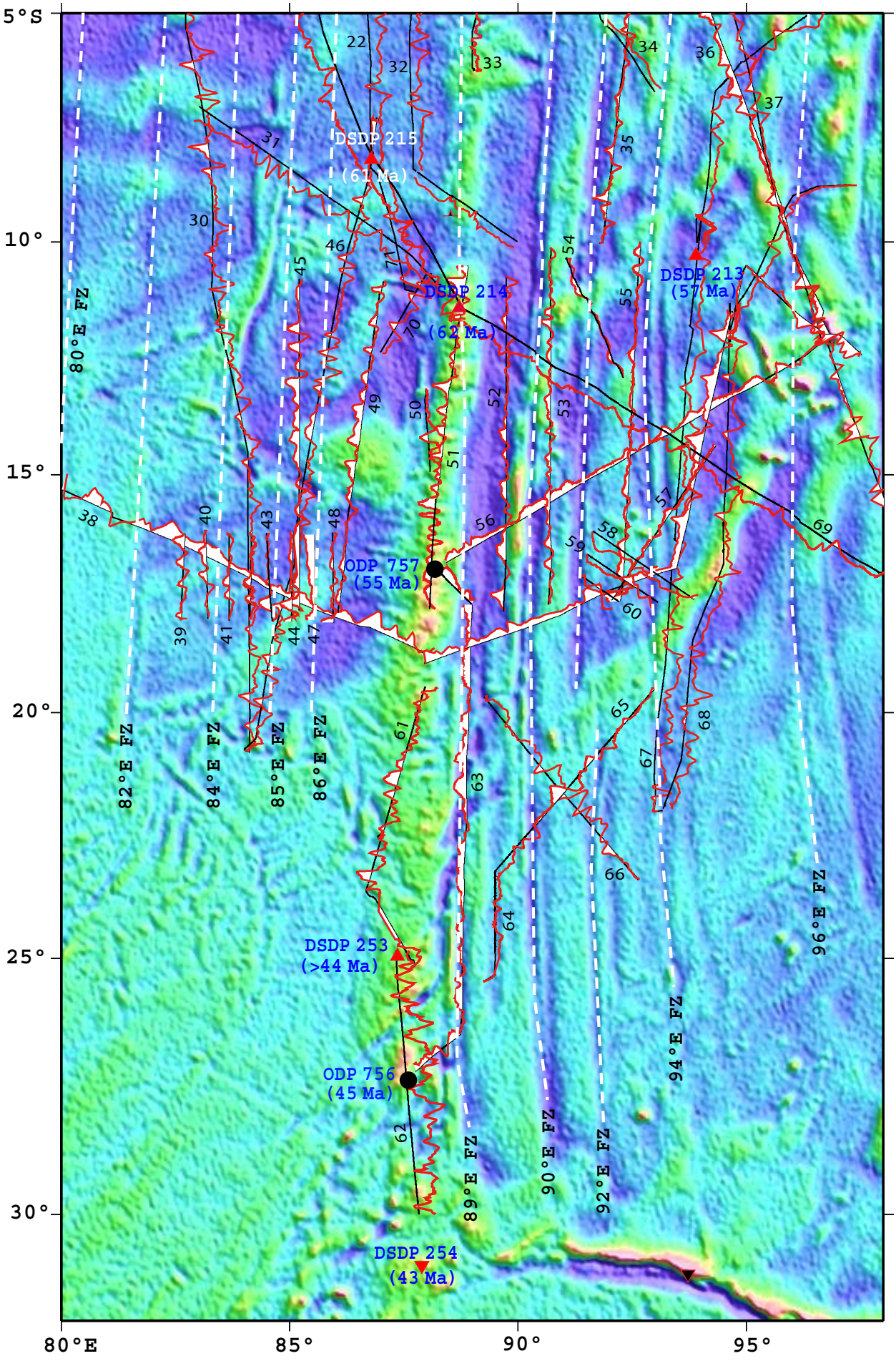
5°S
10°
15°
20°
25°
30°
80°E
85°
90°
95°
80°E FZ
82°E FZ
84°E FZ
85°E FZ
86°E FZ
89°E FZ
90°E FZ
92°E FZ
94°E FZ
96°E FZ
DSDP 215
(61 Ma)
DSDP 214
(62 Ma)
DSDP 213
(57 Ma)
ODP 757
(55 Ma)
DSDP 253
(>44 Ma)
ODP 756
(45 Ma)
DSDP 254
(43 Ma)

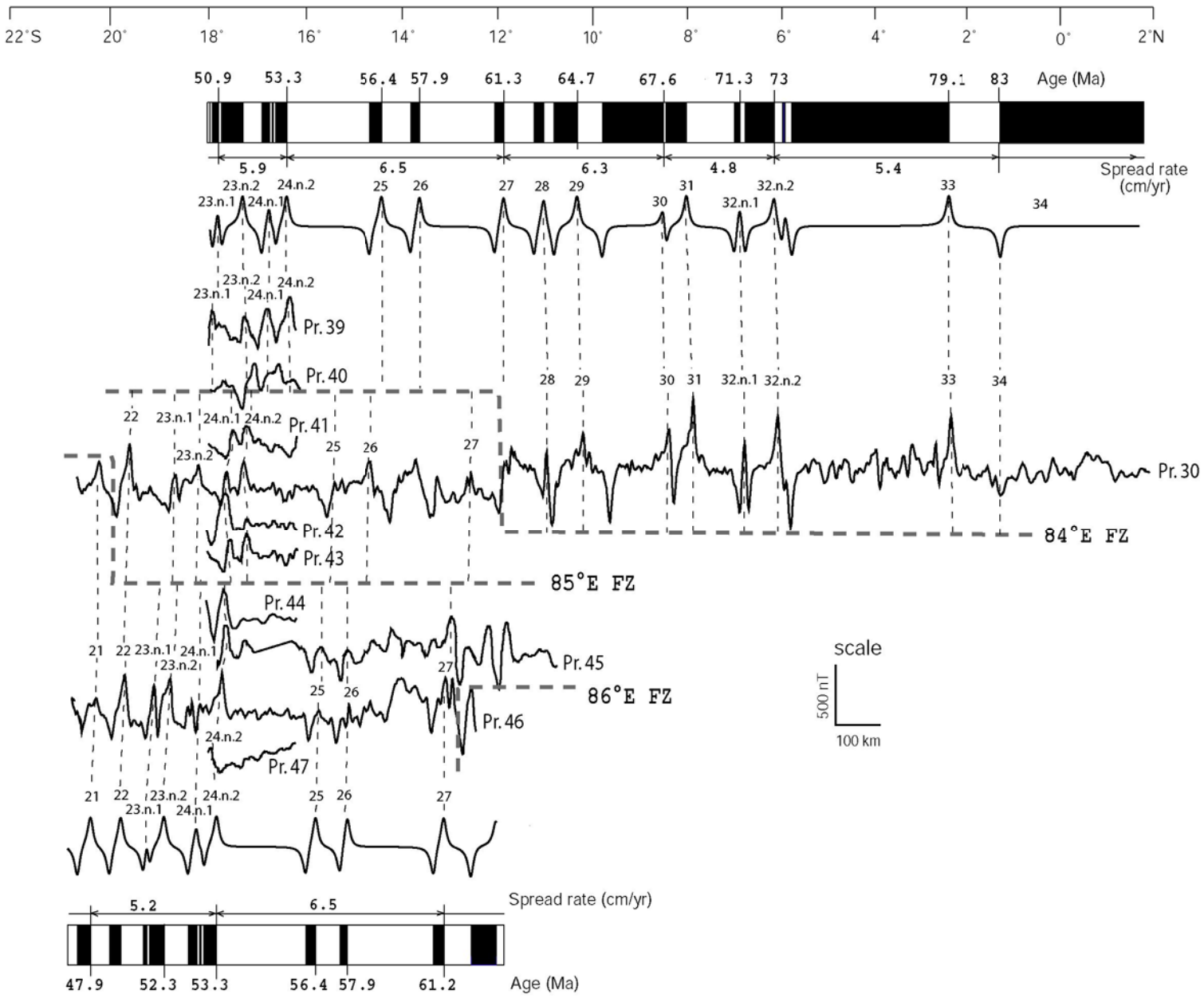
22°S
20°
18°
16°
14°
12°
10°
8°
6°
4°
2°
0°
2°N
50.9
53.3
56.4
57.9
61.3
64.7
67.6
71.3
73
79.1
83
Age (Ma)
5.9
6.5
6.3
4.8
5.4
Spread rate (cm/yr)
23.n.1
23.n.2
24.n.1
24.n.2
Pr. 39
Pr. 40
Pr. 41
Pr. 42
Pr. 43
Pr. 44
Pr. 45
Pr. 46
Pr. 47
Pr. 30
84°E FZ
85°E FZ
86°E FZ
scale
500 nT
100 km
5.2
6.5
47.9
52.3
53.3
56.4
57.9
61.2
Spread rate (cm/yr)
Age (Ma)

Figure 4a

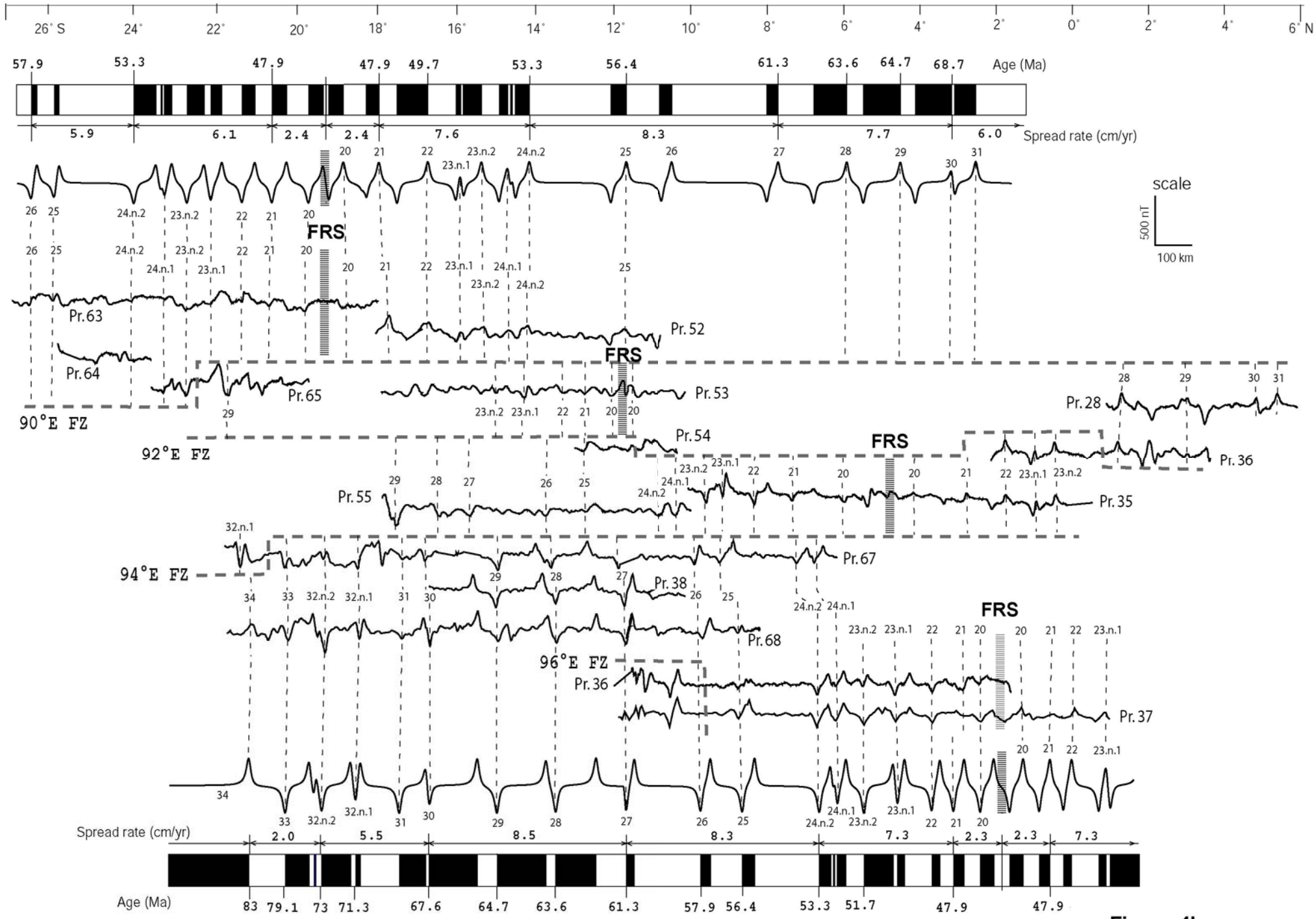
26° S
24°
22°
20°
18°
16°
14°
12°
10°
8°
6°
4°
2°
0°
2°
4°
6° N
57.9
53.3
47.9
47.9
49.7
53.3
56.4
61.3
63.6
64.7
68.7
Age (Ma)
5.9
6.1
2.4
2.4
7.6
8.3
7.7
6.0
Spread rate (cm/yr)
scale
500 nT
100 km
FRS
Pr. 63
Pr. 64
Pr. 65
Pr. 52
Pr. 53
Pr. 54
Pr. 55
Pr. 67
Pr. 38
Pr. 68
Pr. 36
Pr. 37
Pr. 35
Pr. 28
90°E FZ
92°E FZ
94°E FZ
96°E FZ
Spread rate (cm/yr)
2.0
5.5
8.5
8.3
7.3
2.3
2.3
7.3
Age (Ma)
83
79.1
73
71.3
67.6
64.7
63.6
61.3
57.9
56.4
53.3
51.7
47.9
47.9

Figure 4b

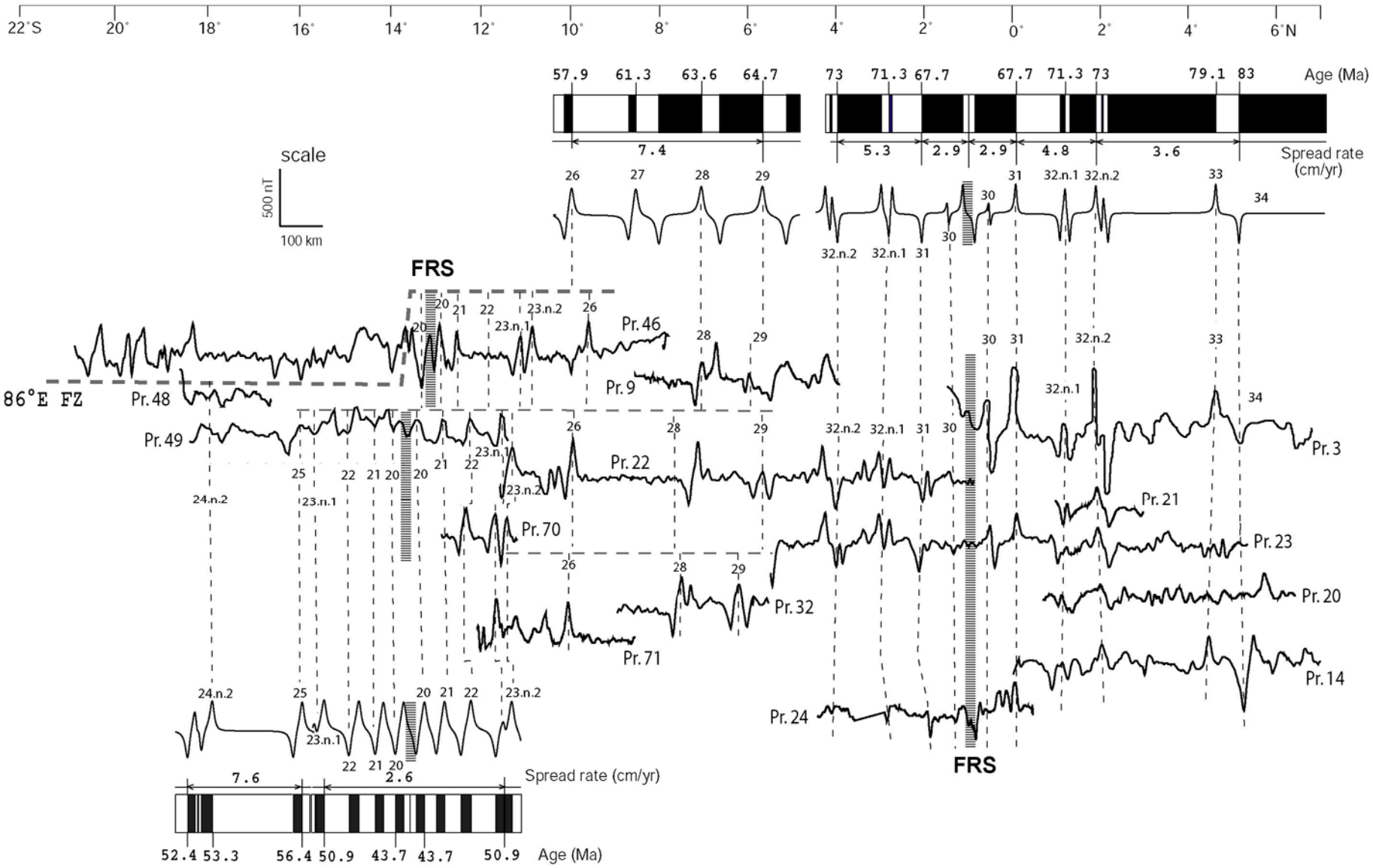
22°S
20°
18°
16°
14°
12°
10°
8°
6°
4°
2°
0°
2°
4°
6°N
57.9 61.3 63.6 64.7
73 71.3 67.7 67.7 71.3 73 79.1 83
Age (Ma)
7.4
5.3 2.9 2.9 4.8 3.6
Spread rate (cm/yr)
scale
500 nT
100 km
FRS
86°E FZ
Pr. 46
Pr. 48
Pr. 9
Pr. 49
Pr. 22
Pr. 3
Pr. 21
Pr. 70
Pr. 23
Pr. 32
Pr. 20
Pr. 71
Pr. 14
Pr. 24
FRS
7.6
2.6
Spread rate (cm/yr)
52.4 53.3 56.4 50.9 43.7 43.7 50.9
Age (Ma)

Figure 4c

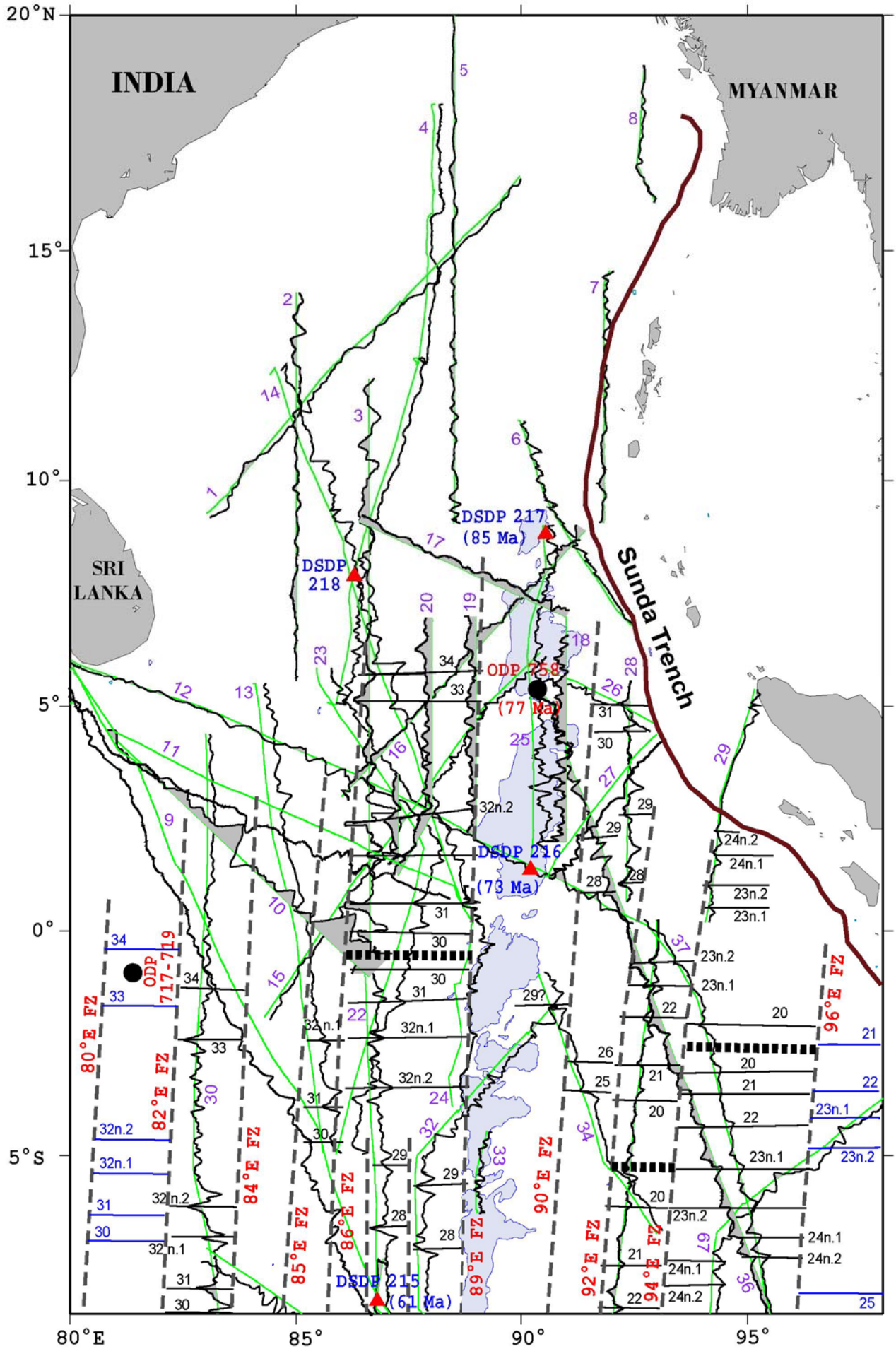
INDIA
MYANMAR
SRI LANKA
Sunda Trench
DSDP 217 (85 Ma)
DSDP 218
ODP 758 (77 Ma)
DSDP 216 (73 Ma)
DSDP 215 (61 Ma)
ODP 717-719
80°E FZ
82°E FZ
84°E FZ
85°E FZ
86°E FZ
89°E FZ
90°E FZ
92°E FZ
94°E FZ
96°E FZ
20°N
15°
10°
5°
0°
5°S
80°E
85°
90°
95°

Figure 5a

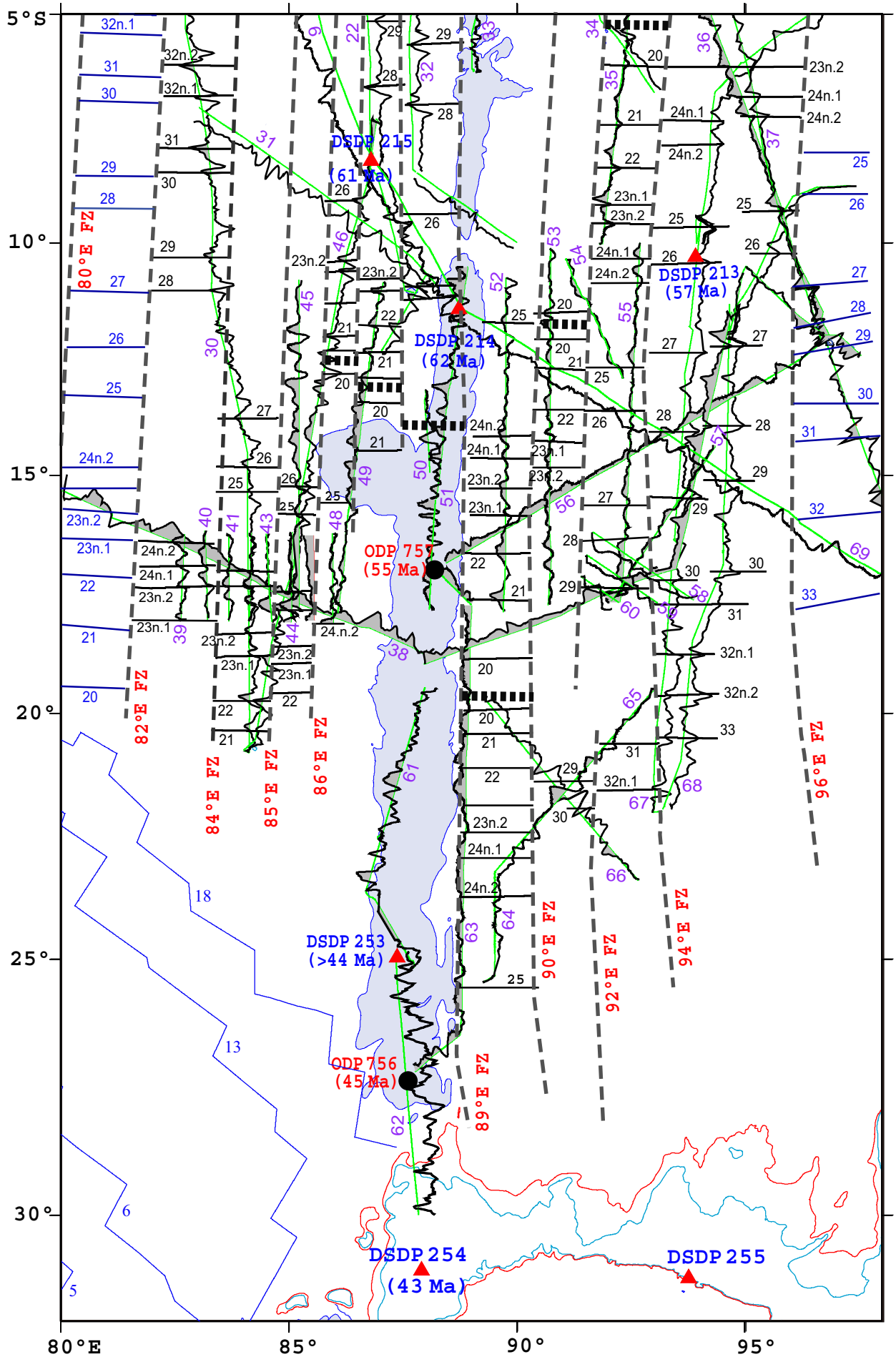
5°S
10°
15°
20°
25°
30°
80°E
85°
90°
95°
80°E FZ
82°E FZ
84°E FZ
85°E FZ
86°E FZ
89°E FZ
90°E FZ
92°E FZ
94°E FZ
96°E FZ
DSDP 215
(61 Ma)
DSDP 214
(62 Ma)
DSDP 213
(57 Ma)
ODP 757
(55 Ma)
DSDP 253
(>44 Ma)
ODP 756
(45 Ma)
DSDP 254
(43 Ma)
DSDP 255

Figure 5b

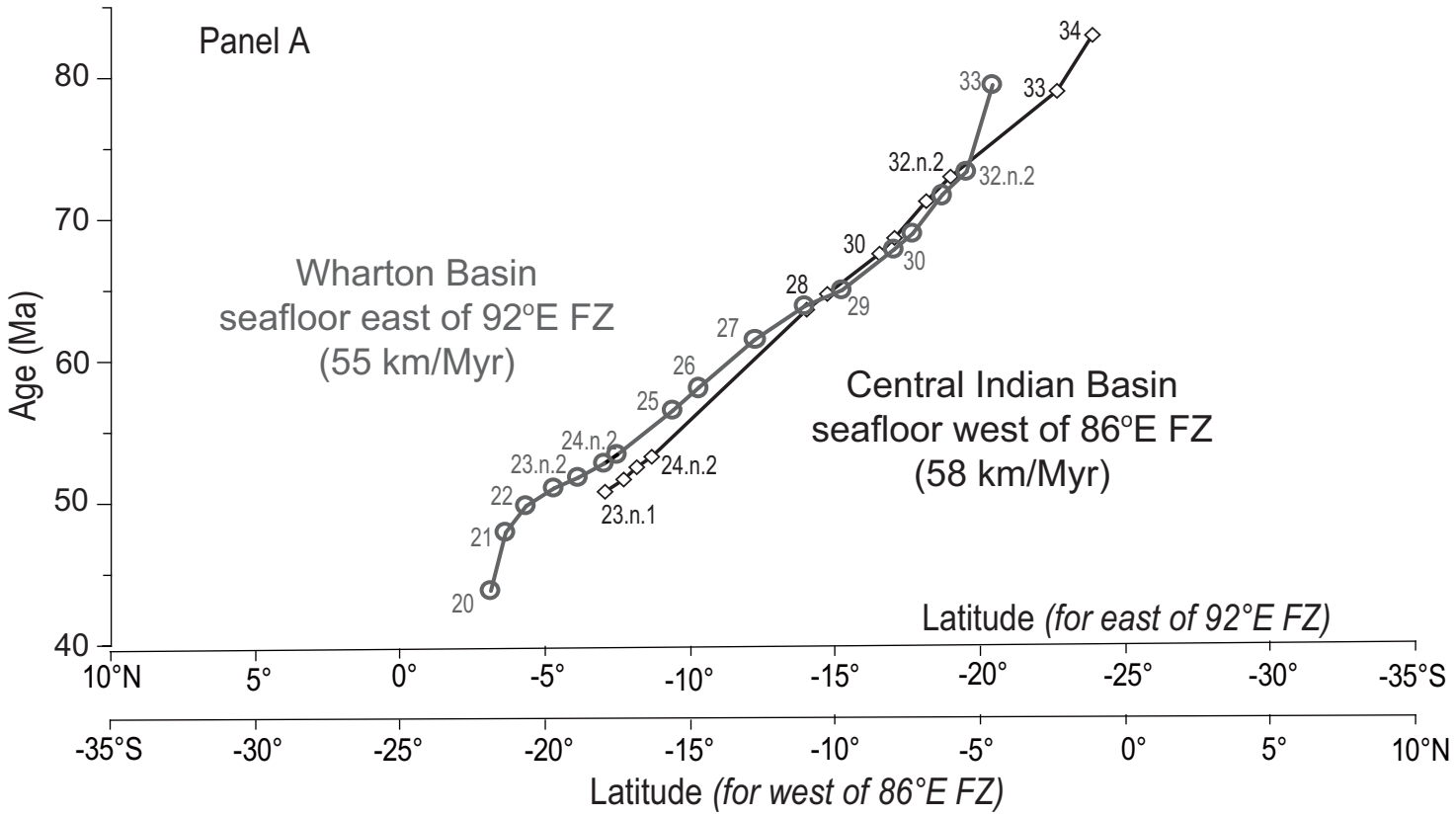
Panel A
Age (Ma)
80
70
60
50
40
Wharton Basin
seafloor east of 92°E FZ
(55 km/Myr)
Central Indian Basin
seafloor west of 86°E FZ
(58 km/Myr)
34
33
33
32.n.2
32.n.2
30
30
28
29
27
26
25
24.n.2
23.n.2
22
21
20
24.n.2
23.n.1
Latitude (for east of 92°E FZ)
10°N
5°
0°
-5°
-10°
-15°
-20°
-25°
-30°
-35°S
-35°S
-30°
-25°
-20°
-15°
-10°
-5°
0°
5°
10°N
Latitude (for west of 86°E FZ)

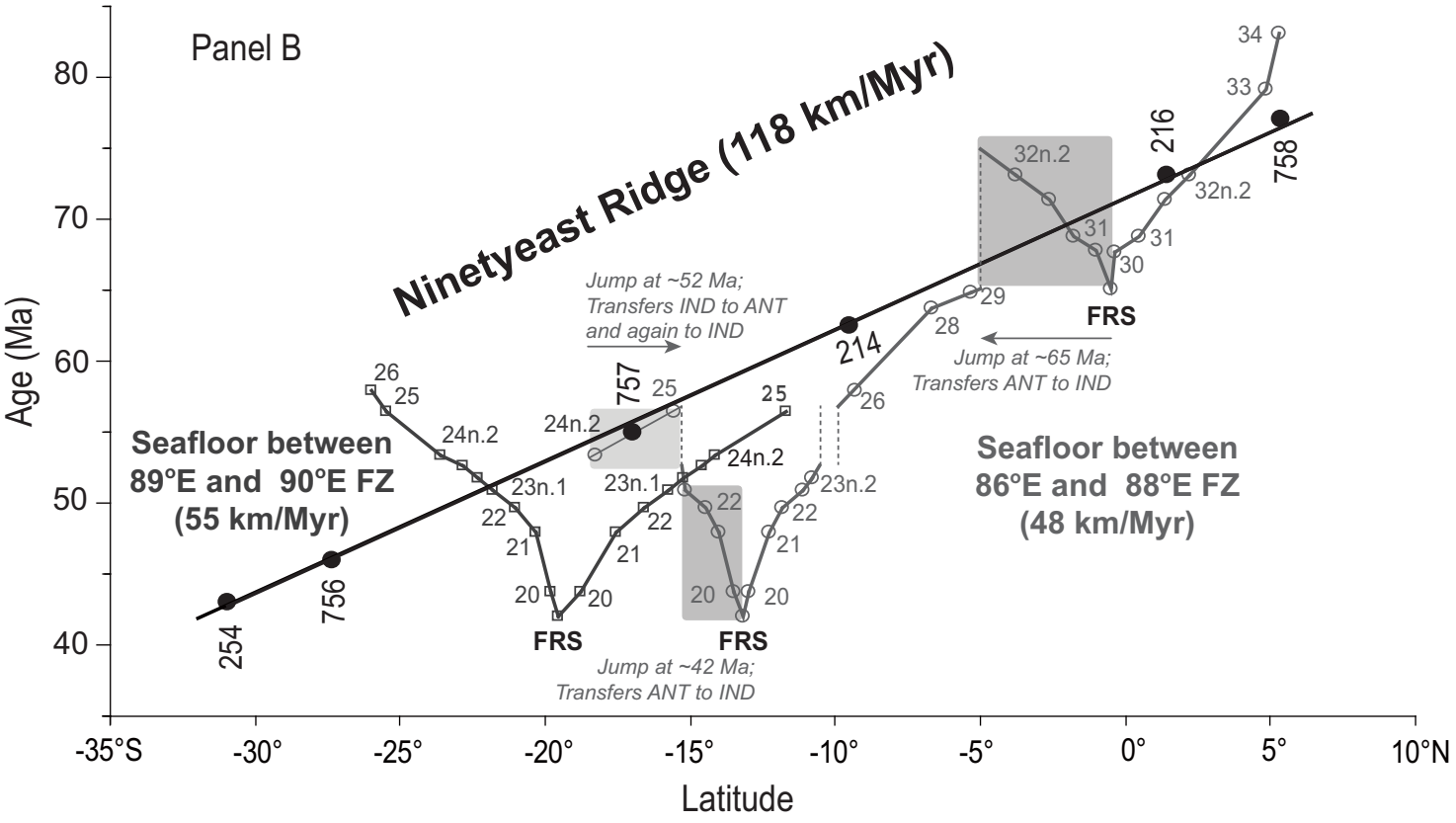
Panel B
Age (Ma)
80
70
60
50
40
Ninetyeast Ridge (118 km/Myr)
Jump at ~52 Ma;
Transfers IND to ANT
and again to IND
Jump at ~65 Ma;
Transfers ANT to IND
Jump at ~42 Ma;
Transfers ANT to IND
FRS
FRS
FRS
Seafloor between
89°E and 90°E FZ
(55 km/Myr)
Seafloor between
86°E and 88°E FZ
(48 km/Myr)
254
756
757
214
216
758
34
33
32n.2
32n.2
31
31
30
29
28
26
25
24n.2
23n.1
22
21
20
25
24n.2
23n.1
22
21
20
26
23n.2
22
21
20
Latitude
-35°S
-30°
-25°
-20°
-15°
-10°
-5°
0°
5°
10°N

Figure 6

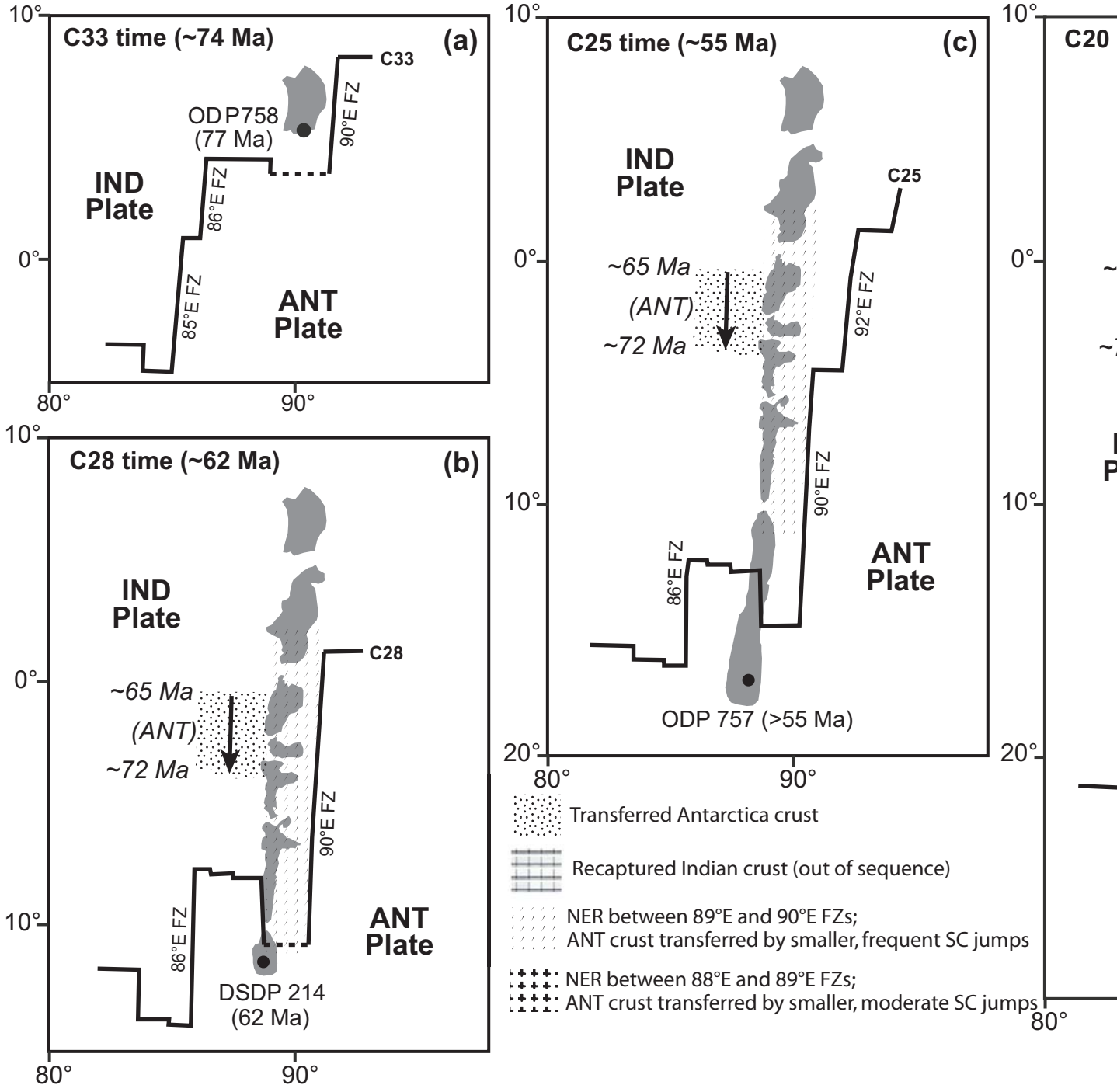
C33 time (~74 Ma)
(a)
C33
ODP758
(77 Ma)
90°E FZ
86°E FZ
85°E FZ
IND
Plate
ANT
Plate
10°
0°
80°
90°
C28 time (~62 Ma)
(b)
IND
Plate
C28
~65 Ma
(ANT)
~72 Ma
90°E FZ
86°E FZ
ANT
Plate
DSDP 214
(62 Ma)
10°
0°
80°
90°
C25 time (~55 Ma)
(c)
IND
Plate
C25
~65 Ma
(ANT)
~72 Ma
92°E FZ
90°E FZ
86°E FZ
ANT
Plate
ODP 757 (>55 Ma)
10°
0°
10°
20°
80°
90°
C20
10°
0°
10°
20°
80°
Transferred Antarctica crust
Recaptured Indian crust (out of sequence)
NER between 89°E and 90°E FZs;
ANT crust transferred by smaller, frequent SC jumps
NER between 88°E and 89°E FZs;
ANT crust transferred by smaller, moderate SC jumps

Figure 7

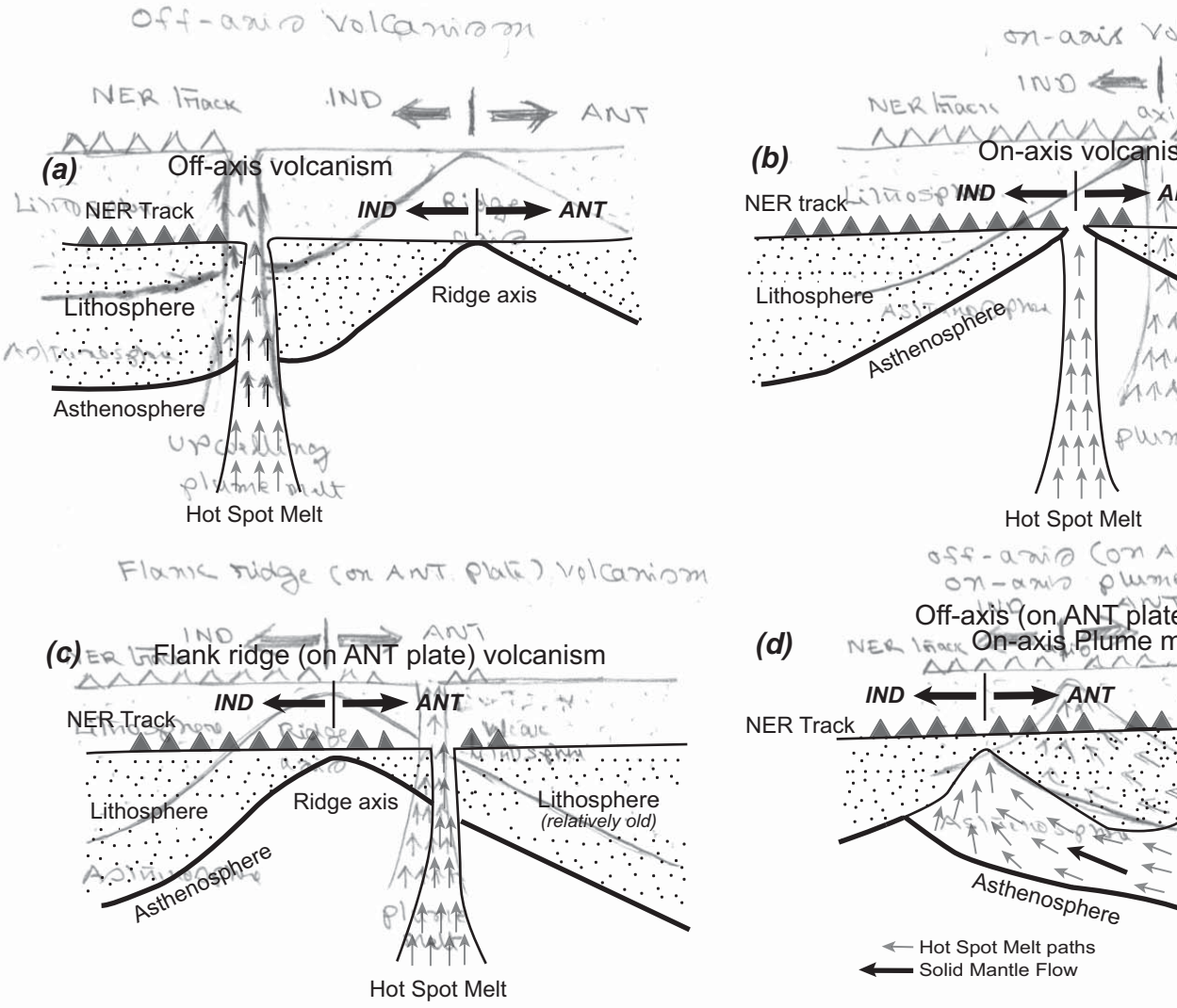
(a)
Off-axis volcanism
NER Track
IND
ANT
Lithosphere
Asthenosphere
Ridge axis
Hot Spot Melt
(b)
On-axis volcanis
NER track
IND
Lithosphere
Asthenosphere
Hot Spot Melt
(c)
Flank ridge (on ANT plate) volcanism
NER Track
IND
ANT
Lithosphere
Ridge axis
Lithosphere
(relatively old)
Asthenosphere
Hot Spot Melt
(d)
Off-axis (on ANT plate
On-axis Plume m
NER Track
IND
ANT
Asthenosphere
Hot Spot Melt paths
Solid Mantle Flow

Figure 8

Table 1: Details of profiles ids and data bases used in the present study

Profile Number used in the present study	Original Profile id	Research vessel used for the data acquisition	Data Source
1	CIRC03AR	R/V Argo	NGDC
2	SK82- 14	ORV Sagar Kanya	NIO database
3	SK82-02	ORV Sagar Kanya	NIO database
4	ANTP11MV	R/V Melville	NGDC
5	SK100-10	ORV Sagar Kanya	NIO database
6	CIRC03AR	R/V Argo	NGDC
7	SK100-20	ORV Sagar Kanya	NIO database
8	CIRC03AR	R/V Argo	NGDC
9	WILKES815	USNS Wilkes	NGDC
10	SK82-01	ORV Sagar Kanya	NIO database
11	WILKES907	USNS Wilkes	NGDC
12	C0909	R/V Conrad	NGDC
13	C0909	R/V Conrad	NGDC
14	INMDO6MV	R/V Melville	NGDC
15	CIRC03AR	R/V Argo	NGDC
16	SK100-01c	ORV Sagar Kanya	NIO database
17	SK124-5	ORV Sagar Kanya	NIO database
18	SK124-6	ORV Sagar Kanya	NIO database
19	SK124-8	ORV Sagar Kanya	NIO database
20	SK124-10	ORV Sagar Kanya	NIO database
21	SK124-12	ORV Sagar Kanya	NIO database
22	DSDP22GC	R/V Glomar Challenger	NGDC
23	C1709	R/V Conrad	NGDC
24	WILKES907	USNS Wilkes	NGDC
25	CIRC03AR	R/V Argo	NGDC
26	RC1402	R/V Robert Conrad	NGDC
27	DSDP22GC	R/V Glomar Challenger	NGDC
28	8400121b	R/V Jean Charcot	NGDC
29	LUSI7BAR	R/V Argo	NGDC
30	CIRC05AR	R/V Argo	NGDC
31	RC1402	R/V Robert Conrad	NGDC
32	RC1402	R/V Robert Conrad	NGDC
33	KNOX06RR	R/V Roger Revelle	NGDC
34	INMDO6MV	R/V Melville	NGDC
35	8400121a	R/V Jean Charcot	NGDC
36	ODP121JR	Joides Resolution	NGDC
37	C0909	R/V Conrad	NGDC
38	MONS3AR	R/V Argo	NGDC

39	TIOG-7	R/V Issledovatl	ILTP database
40	TIOG-8	R/V Issledovatl	ILTP database
41	TIOG-9	R/V Issledovatl	ILTP database
42	TIOG-10	R/V Issledovatl	ILTP database
43	TIOG-11	R/V Issledovatl	ILTP database
44	TIOG-12	R/V Issledovatl	ILTP database
45	TIOG-13	R/V Issledovatl	ILTP database
46	CIRC05AR-B	R/V Argo	NGDC
47	TIOG-14	R/V Issledovatl	ILTP database
48	TIOG-15	R/V Issledovatl	ILTP database
49	TIOG-16	XVII Syezo Profsoyuzov	ILTP database
50	KNOX06RR	R/V Roger Revelle	NGDC
51	TIOG-17	XVII Syezo Profsoyuzov	ILTP database
52	TIOG-18	XVII Syezo Profsoyuzov	ILTP database
53	TIOG-19	XVII Syezo Profsoyuzov	ILTP database
54	TIOG-20	XVII Syezo Profsoyuzov	ILTP database
55	TIOG-21	XVII Syezo Profsoyuzov	ILTP database
56	ODP121JR	Joides Resolution	NGDC
57	TIOG-51	XVII Syezo Profsoyuzov	ILTP database
58	TIOG-60	XVII Syezo Profsoyuzov	ILTP database
59	TIOG-61	XVII Syezo Profsoyuzov	ILTP database
60	TIOG-62	XVII Syezo Profsoyuzov	ILTP database
61	KNOX06RR	R/V Roger Revelle	NGDC
62	DSDP26GC	R/V Glomar Challenger	NGDC
63	ODP121JR	Joides Resolution	NGDC
64	KNOX06RR	R/V Roger Revelle	NGDC
65	KNOX06RR	R/V Roger Revelle	NGDC
66	CIRC05AR	R/V Argo	NGDC
67	ANTP12MVa	R/V Melville	NGDC
68	ANTP12MVb	R/V Melville	NGDC
69	WILKES815	USNS Wilkes	NGDC
70	CIRC05AR-C	R/V Argo	NGDC
71	WILKES907	USNS Wilkes	NGDC